2008

Sediment Transport and Erodibility in the York River Estuary: A Model Study

Jeffrey Paul Rinehimer
College of William and Mary - Virginia Institute of Marine Science

SEDIMENT TRANSPORT AND ERODIBILITY IN THE YORK RIVER ESTUARY: A MODEL STUDY

A Thesis

Presented to

The Faculty of the School of Marine Science

College of William and Mary

In Partial Fulfillment

Of the Requirements for the Degree of

Masters of Science

---

by

Jeffrey Paul Rinehimer

2008

APPROVAL SHEET

This thesis is submitted in partial fulfillment of

the requirements for the degree of

Master of Science

J. Paul Rinehimer

Approved, by the Committee, October 2008

Courtney K. Harris, Ph.D.
Advisor

Carl T. Friedrichs, Ph.D.

Harry V. Wang, Ph.D.

Linda C. Schaffner, Ph.D.

L. Donelson Wright, Ph.D.

CONTENTS

ACKNOWLEDGMENTS

I would like to thank my major adviser, Courtney Harris, without whose guidance, support, and patience this project would not have been possible. The thoughtful input of the other committee members was also greatly appreciated. Chris Sherwood (USGS) is primarily responsible for implementing the CSTMS cohesive sediment bed model while input from Larry Sanford (UMCES) and Benedicte Ferre (USGS) help guide my efforts. Sherwood and Sanford also provided advice and support while publishing the second chapter. Jae-Il Kwon graciously provided his York River model grid for adaptation to ROMS. Mary Ann Bynum, Adam Miller, Chris Bording, and Dale Castle provided support with the High Performance Cluster at VIMS. Pat Dickhudt and Grace Carwright helped to ground the model in reality by allowing me to use their observational data.

Development of the CSTMS was supported by the US Geological Survey and the National Oceanographic Partnership Program (NOPP). This work was part of the Multidisciplinary Benthic Exchange Dynamics (MUDBED) project supported by funding from the National Science Foundation Coastal Ocean Processes (CoOP) program (Grant #OCE-0536572).

LIST OF FIGURES

ABSTRACT

A cohesive sediment bed model was implemented in the Community Sediment Transport Modeling System (CSTMS) to examine processes influencing sediment erodibility and suspended sediment concentrations. Estimates of eroded mass from the sediment bed model were calibrated and verified with erosion chamber measurements from the York River, Virginia, a tidally-dominated environment. A constant erosion rate parameter combined with depth-varying critical shear stress was sufficient to model erosion observations of depth-limited sediment cores. Sensitivity of total eroded mass to seasonal variations in erodibility and changes in consolidation time scale was evaluated during spring-neap variations in bottom stresses. Differences were greatest during spring tide and varied by as much as a factor of 2.5. Consolidation created an asymmetry between the spring-to-neap and neap-to-spring transitions with more sediment being eroded during the decreasing phase of maximum tidal stress. Consolidation time scales controlled the magnitude of this asymmetry with larger asymmetries occurring when slower consolidation time scales were assumed. Eroded mass estimates were potentially as sensitive to uncertainties in the consolidation time scale as they were to observed seasonal variability in critical stress.

The cohesive sediment bed model was then implemented within a numerical model of the York River Estuary to examine feedbacks between sediment flux convergence and erodibility. Model results show the development of a highly erodible pool of sediment near the ETM location. Even when sediment convergence processes were diminished, suspended sediment concentrations remain high due to high sediment erodibility. Sediment concentrations and erodibility exhibited high spatial variability in both the along and across channel directions. As opposed to the results of the one-dimensional model, sediment concentrations and erodibility estimates were less sensitive to variations in the consolidation rate than to the initial bed conditions. Model calculations of sediment concentrations and erodibility showed similar patterns to observational data.

SEDIMENT TRANSPORT AND ERODIBILITY IN THE YORK RIVER ESTUARY: A MODEL STUDY

CHAPTER 1

Introduction

Sediment transport is an important process in the marine environment, impacting carbon, nutrient, and contaminant transport and sequestration; biological productivity; and maritime navigation. Suspended particulates attenuate light and limit primary productivity, altering marine ecosystems (Dennison et al., 1993; Koch, 2001). As sediments accumulate in important navigational waterways, repeated dredging of channels is often required. Also, sediment resuspension can control the dispersal of contaminants sorbed onto sediment particles (Sherwood et al., 2002b; Wiberg and Harris, 2002). Cohesive sediments, generally of clay and silt size, tend to adhere together forming high water content aggregates that consolidate after deposition on the seabed (Winterwerp and van Kesteren, 2004). Additionally, benthic organisms can rework, stabilize, or destabilize the bed, altering its physical properties (Boudreau and Jorgensen, 2001). The cohesive nature of muddy estuarine sediment presents challenges in predicting suspended sediment concentrations in these systems.

The fate of sediment eroded from the bed or transported into an estuary from external sources is controlled by the hydrodynamics of the system and the particle settling velocity, w_s. Cohesive particles traveling as aggregates will have settling velocities one or two orders of magnitude larger than their disaggregated constituents (Hill and McCave, 2001). Spatial and temporal variability of suspended

sediment concentrations respond to a number of factors including sediment loading from rivers, local erosion (Lin and Kuo, 2003), and convergence due to gravitational circulation (Festa and Hansen, 1978), damping of turbulence by stratification (Geyer, 1993) or tidal asymmetry (Jay and Musiak, 1994). In a real estuary, these processes are inherently three-dimensional and time dependent and are difficult to study using field methods alone due to the intensive amount of work required to adequately sample the system. Three-dimensional numerical models, however, can be used to evaluate the effects of bed properties and hydrodynamic controls on sediment transport while interpolating gaps in field measurements.

Sediment erodibility is an important factor in determining suspended sediment concentrations. Erodibility is generally quantified by τ_{cr}, the critical bed shear stress necessary to erode sediment. Within the upper few millimeters of the bed τ_{cr} increases greatly with depth, mainly due to self-weight consolidation (Parchure and Mehta, 1985). Factors such as particle size distribution (Roberts et al., 1998), reworking by benthic organisms (Black, 1997; Boudreau and Jorgensen, 2001), and the recent erosional and depositional history can influence τ_{cr}. Extensive field measurements using devices such as the Gust Microcosm (Gust and Muller, 1997) may be used to determine bed erodibility for a site due to these complications.

The York River, VA (Figure 1.1) provides an excellent laboratory for modeling cohesive sediment processes in the water column and the seabed. The results of previous work characterizing hydrodynamics, sediment dynamics, depositional geology and benthic biology provide a solid foundation for research (Lin and Kuo, 2001; Schaffner et al., 2001; Dellapenna et al., 2003; Scully et al., 2003; Scully and Friedrichs, 2007). This study has been part of the Multidisciplinary Benthic Exchange Dynamics (MUDBED) project which has examined the interactions between physical and biological controls on cohesive sediment transport and deposition within the York River. This thesis explores the feedbacks between suspended sedi-

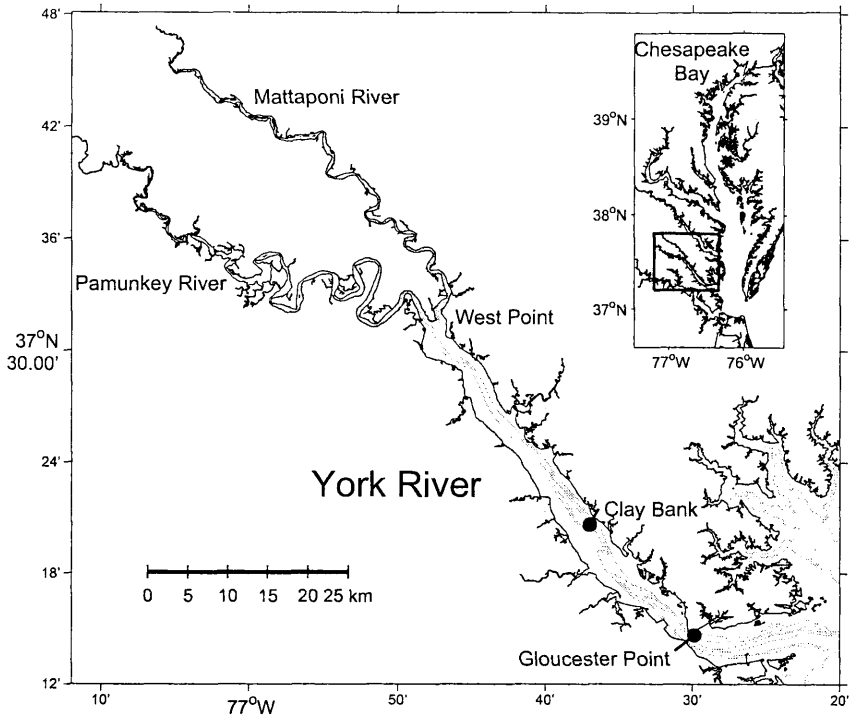

Figure 1.1: York River, Virginia, USA. Light contours are bathymetry in 5 m intervals The study locations at Clay Bank and Gloucester point are marked. Inset map shows location of the York River within the Chesapeake Bay

ment dynamics and erodibilitiy within the York River by developing a bed consolidation model, testing the model sensitivity to seabed and consolidation parameters, and then applying the seabed model within a numerical, three-dimensional, hydrodynamic model of the river.

1.1 Study Site

The York River is a drowned river valley estuary formed about 7,000 years ago as sea levels rose at the end of the Pleistocene. The river is a net sediment sink for both riverine and marine sediment. Order-of-magnitude estimates show that, for the modern system, about 55% of the sediment is from the Pamunkey and Mattaponi

watersheds and 32% is from the Chesapeake Bay and marine sources (Nichols et al., 1991). The remaining 13% is from shoreline erosion. Bottom sediments are predomantly muddy, but sandy regions are located along the shoals flanking the main river channel (Dellapenna et al., 2003).

The York River Estuary is a partially-mixed microtidal estuary with a typical tidal range of 0.7 m at the mouth and 1 m at the head (Schaffner et al., 2001). It forms at the confluence of the Mattaponi and the Pamunkey Rivers at West Point, Virginia. Between West Point and Gloucester Point, a distance of about 40 km, the estuary is straight and consists of a 5-10 m deep channel with 2 m deep shoals on either side. At Gloucester Point, the river turns toward the north, widens from 3 to 6 km, and the channel depth increases to 20 m with a broad northern shoal and a narrow southern shoal. This configuration divides the river into two regimes: the broad, deep, exposed lower river, where resuspension of sediment is likely driven by waves during storms, and the narrow, shallow upper river dominated by tidal currents (Dellapenna et al., 2003). Due to the more intense tidal currents, a greater range of salinities, and the ephemeral presence of a secondary turbidity maximum (STM) in the upper river, benthic biology there is constrained (Schaffner et al., 2001). Physical processes like erosion and deposition during tidal cycles likely control critical shear stresses of the bed in this region. Tidal currents in the lower, deeper river are generally less intense and the bed is disturbed only during storms. Because of the less frequent occurrence of bed disturbance, sediment dynamics in the lower river likely reflect biologic control through biostabilization, biodestabilization, and bioturbation.

Lin and Kuo 2001 observed an STM about 40 km from the mouth in the transition region between a well-mixed and stratified water column. They concluded that the STM was maintained by sediment resuspension and turbulence damping in the transition zone due to salinity stratification. Using the numerical Hydrodynamic

Eutrophication Model (HEM-3D)(Park et al., 1995) they were able to simulate the spatial locations of the turbidity maxima, but the magnitude of the simulated results were only 40 mgL^{-1}, a factor of 2.5 lower than the observed concentrations of 100 mgL^{-1} (Lin and Kuo, 2003). Their model, however, used only a constant value of critical shear stress ($\tau_c = 0.1Pa$) and a limited bed sediment supply determined by initializing the bed with deposited sediment thickness of a prior model case. Incorporating spatial variability of erosion rates, Kwon (2005) was able to reduce errors in bottom suspended sediment concentrations by 55%. Without simulating the feedbacks between sediment depostion and erosion, their models may not recreate a pool of highly erodible sediment in the vicinity of the STM. Results from radioisotope (^{210}Pb) studies suggest that physical mixing depths in this region are around 40 to 120 cm while x-radiographs show little evidence of bioturbation, indicating active resuspension and deposition processes over seasonal to decadal timescales (Dellappenna et al., 1998). Further observations revealed century-scale residence times for particles in the physical mixed layer while the mass of sediment in the layer was equivalent to approximately 70 years of river sediment yield (Dellapenna et al., 2003).

Biological activity in the study area follows a gradient from the upper York River to the Chesapeake Bay with abundance and species richness increasing downriver (Schaffner et al., 2001). While the species in the upper river are active bioturbators, the influence of benthic organisms is overwhelmed by physical mixing due to sediment resuspension and deposition (Dellappenna et al., 1998). Toward the river mouth and the Chesapeake Bay, bioturbation rates are greatest and exhibit seasonal variation (Schaffner et al., 1997). Biological pelletization of cohesive sediment, which can increase settling velocities by aggregation (Drake et al., 2002), also increases toward the river mouth (Fugate and Friedrichs, 2003).

1.2 Objectives

As its main objective, this research examined the importance of variations in bed erodibility, both physical and biological in origin, in determining turbidity in a muddy estuarine environment. The York River Estuary was used as a case study to capitalize on efforts from the Multidisciplinary Benthic Exchange Dynamics (MudBED) project. The research questions were as follows:

1. *Sensitivity to Forcing and Bed Parameters:*

   Do seasonal changes in critical stress profiles and consolidation rates control sediment resuspension under typical estuarine hydrodynamic conditions like semi-diurnal, spring-neap tides? (Chapter 2)

2. *Importance of Local Erosion:*

   How do variations in erodibility interact with the spatial variability of suspended sediment concentrations and depositional patterns that are also influenced by flux convergence and sediment loading typical of the York River? (Chapter 3)

3. *Importance of Spatial and Seasonal Variations:*

   To what extent do hydrodynamics control bed erodibility? Can physical redistribution of sediments explain observed seasonal or spatial erodibility patterns? (Chapter 3)

In Chapter 2, the results of tests of a one dimensional cohesive sediment bed model are presented. The bed model includes depth and time dependent variations in critical shear stress due to consolidation (Sanford, 2008), but using a constant erosion rate parameter. The model was tested both by simulating erosion chamber experiments and by running sensitivity tests using spring-neap tidal forcing typical of the York River. Two sets of sensitivity tests were run to determine how erodibility

parameters affect estimates of eroded mass. In the first, the depth-dependent critical stresses were varied by using erosion chamber data from April and September, 2007 to investigate how total eroded mass depended on seasonal variations in erodibility. In the second set of tests, the importance of consolidation was determined by varying consolidation timescales.

The results of a three-dimensional modeling study of the York River are presented in Chapter 3. The bed model from Chapter 2 was included in the Regional Ocean Modeling System (ROMS). The first 200 days of 2007 were simulated to determine how sediment convergence processes that lead to ETM formation affect sediment erodibility. Time-series at the study locations were analyzed to determine seasonal changes in suspended sediment concentrations and erodibility at the study sites. Tidally-averaged along- and across-channel transects of model results are presented showing spatial and temporal variability in sediment dynamics. Estimated along-channel fluxes and sediment resuspension show how these factors contribute to the development of the STM. Finally, the sensitivity of the model to consolidation timescale was tested and model results were compared to previous studies of estuarine suspended sediment concentrations and erodibility.

The results of this work contributes significantly to the understanding of cohesive sediment dynamics. The new cohesive sediment bed model used here has been included within the large, open source, Community Sediment Transport Modeling System (CSTMS) (Sherwood et al., 2002a), impacting the sediment modeling and management communities. The model application to the MUDBED study sites is useful for comparing physical reworking of sediment to biological disturbances and additionally allows inferences to be made about the rest of the York River system beyond the study sites. Finally, while the results of the York River model may be specific to this locality, the general processes are likely valid for similar estuarine systems.

CHAPTER 2

Estimating Cohesive Sediment Erosion and Consolidation in a Muddy, Tidally-Dominated Environment: Model Behavior and Sensitivity.[1]

2.1 Abstract

Erodibility of cohesive sediment varies with sediment depth and with erosional and depositional history. A cohesive sediment bed model was implemented in the Community Sediment Transport Modeling System (CSTMS) to examine processes influencing sediment erodibility and water column turbidity. Estimates of eroded mass from the sediment bed model were calibrated and verified with erosion chamber measurements from the York River, Virginia, a tidally-dominated environment. The model performs well when a constant erosion rate parameter is used and critical stress is varied with depth. Sensitivity of total eroded mass to seasonal variations in erodibility and changes in consolidation time scale was evaluated during spring-neap variations in bottom stresses. Differences were greatest during spring tide and varied by as much as a factor of 2.5. Consolidation created an asymmetry between the spring-to-neap and neap-to-spring transitions with more sediment being eroded during the decreasing phase of maximum tidal stress. Consolidation time scales controlled the magnitude of this asymmetry with larger asymmetries occurring

[1]This chapter is published as:
Rinehimer, J.P., C.K. Harris, C.R. Sherwood, and L.P. Sanford, 2008. Estimating cohesive sediment erosion and consolidation in a muddy, tidally-dominated environment: model behavior and sensitivity. Estuarine and Coastal Modeling, Proceedings of the Tenth Conference, November 5-7, Newport RI. Spaulding, M.L., ed. 819-838.

when slower consolidation time scales were assumed. Eroded mass estimates were potentially as sensitive to uncertainties in the consolidation time scale as they were to observed seasonal variability in critical stress.

2.2 Introduction

Erosion of seabed sediment is an important control on turbidity in marine and estuarine environments. Sediment erosion is caused when bottom shear stress τ_b exerted by currents and waves exceeds the critical shear stress for erosion τ_{cr} (Shields, 1936). In non-cohesive sediments consisting of sand and coarse silts, τ_{cr} depends primarily on grain size and increases with grain diameter (Shields, 1936; Wiberg and Smith, 1987). Besides critical shear stress, models of the erodibility of non-cohesive beds have incorporated the concept of bed armoring by including an "active layer" (Wiberg et al., 1994; Harris and Wiberg, 1997).

For fine sediments, however, τ_{cr} does not primarily depend on grain size. Fine silts and clays tend to form cohesive sediment beds within which τ_{cr} increases as a function of depth with a strong gradient at the surface and an asymptotic approach toward a constant value at depth (Parchure and Mehta, 1985; Piedra-Cueva and Mory, 2001). The large increase of τ_{cr} with depth in the upper few centimeters of the bed is mainly due to self-weight consolidation of fine grained sediments. The weight of overlying sediment encourages the de-watering of underlying material and the seabed consolidates as its porosity decreases with time and depth. The rate of consolidation depends upon the pressure of the overlying mass of sediment and the bed sediment concentration. If the overlying sediment mass is eroded the bed will rewater and swell (Winterwerp and van Kesteren, 2004). While bed consolidation can be estimated directly using numerical models (Gibson et al., 1967; Toorman and Berlamont, 1993; Winterwerp and van Kesteren, 2004), the equations are complex

and nonlinear, and they often provide little insight into important parameters for erosion.

Other factors such as particle size distribution (Roberts et al., 1998) and biological effects (Black, 1997) can influence cohesive sediment erodibility in addition to consolidation. Benthic organisms can alter bed consolidation by mixing sediment through bioturbation, by creating macropores through burrowing, or by creating high density fecal pellets (Boudreau and Jorgensen, 2001). Due to these complications, extensive field measurements of bed properties and suspended sediment concentrations are needed to parameterize the erosive behavior of muddy beds. Erosion devices like the Gust Microcosm (Gust and Muller, 1997) can be used to obtain measurements of depth variations in erodibility by subjecting field-collected sediment cores to well calibrated bed shear stresses.

Many 3-D numerical models have used a constant critical shear stress for muddy sediment due to lack of data. (See e.g. Wang and Pinardi, 2002; Lin and Kuo, 2003; Harris et al., 2004). While satisfactory results can be obtained using this simplification over short time scales, it does not adequately represent the various feedbacks that control erodibility over multiple depositional and erosional events. For example, variations in erodibility due to erosion and deposition on various time scales, such as flood events or spring freshet deposits (Sanford et al., 2001; Harris and Wiberg, 2001; Geyer et al., 2001) or biogenic seasonal variations (Stevens et al., 2007) cannot be modeled directly using a constant τ_{cr}.

Researchers have developed several models in their attempts to quantify erosion of cohesive sediments. Erosion equations have been successfully compared with field and lab measurements using exponential (Gularte et al., 1980; Parchure and Mehta, 1985), power-law (Lick, 1982; Maa et al., 1998; Roberts et al., 1998) and linear equations (Sanford and Maa, 2001; Stevens et al., 2007). If, as we argue below, the amount of sediment eroded is primarily limited by availability, results are insensitive

to the exact formulation of erosion rate, so we have adopted the simplest (linear) formula of McLean (1985):

$$E = M(z)(\tau_b - \tau_{cr}(z)) \tag{2.1}$$

where E is the erosion rate ($\mathrm{kg\,m^{-2}\,s^{-1}}$), τ_b is the bed shear stress (Pa), $\tau_{cr}(z)$ is the critical shear stress for erosion (Pa), and $M(z)$ is the erosion rate parameter ($\mathrm{kg\,m^{-2}\,s^{-1}\,Pa^{-1}}$) and z is depth into the sediment bed. This approach fits lab and field data well and uses only two, depth-dependent empirical parameters, τ_{cr} and M (McLean, 1985; Sanford and Maa, 2001). In Baltimore Harbor, Maryland, Sanford and Maa (2001) found that values of τ_{cr} and M are on the order of $\tau_{cr} = 0.1\,\mathrm{Pa}$ and $M = 20\,\mathrm{kg\,m^{-2}\,s^{-1}\,Pa^{-1}}$ for unconsolidated sediment near the surface and $\tau_{cr} = 0.4\,\mathrm{Pa}$ and $M = 70\,\mathrm{kg\,m^{-2}\,s^{-1}\,Pa^{-1}}$ for consolidated sediment at depth. Generally, recently deposited, unconsolidated sediment will have low values of τ_{cr} and M while sediment that has been allowed to consolidate will have much higher values. Both τ_{cr} and M are site-specific and may vary seasonally so that field observations are needed to apply Eq. 2.1. These depth, temporal, and spatial variations in both M and τ_{cr} are important for limiting sediment supply, but they have only recently been included in numerical modeling efforts (Sanford, 2008), and this treatment has not been applied to many field locations.

Cohesive sediment erosion can be classified as depth limited (Type I) when the gradient of critical stress with depth $d\tau_{cr}/dz$ is important for controlling erosion. The magnitude of M determines erosion during rate limited (Type II) conditions when M is small or τ_{cr} is constant with depth. The amount of time during which a bed stress is applied can also influence whether erosion is rate or depth limited. A constant bed stress τ_b applied over a long period of time erodes all available sediment above the depth z where $\tau_{cr}(z) = \tau_b$, resulting in depth-limited erosion. When the time scale of stress forcing is small, rate-limited erosion occurs because available

sediment has not been completely removed from the bed.

The importance of depth versus rate limitation under oscillatory forcing with a radian frequency ω, can be evaluated using the nondimensional erosion type parameter p^2. Following Sanford and Maa (2001),

$$p^2 = \left(\frac{M \frac{d\tau_{cr}}{dm}}{2\omega} \right)^2 \tag{2.2}$$

where $d\tau_{cr}/dm$ is the critical stress gradient in the bed and the vertical bed coordinate z has been replaced with a mass-depth coordinate m, i.e. the total bed mass above z. Mass-depth m is defined as

$$m(z) = \int_0^z \rho_s \phi_s(\zeta) d\zeta \tag{2.3}$$

where ρ_s is the sediment density, ϕ_s is the solids fraction, and ζ is an integration variable. When $p^2 = 1$, the erosion rate and the gradient of critical stress are of equal importance in controlling erosion. For $p^2 \gg 1$ erosion is depth limited (Type I) and the critical stress profile controls the amount of sediment eroded while for $p^2 \ll 1$ erosion is rate limited (Type II) and the erosion rate parameter is the important factor determining erosion.

Another approach to modeling bed consolidation has used bed layers with defined ages (Gailani et al., 1991; Lick et al., 1994). The numerical model ECOM-SED (HydroQual, Inc, 2002) follows this approach where each layer is defined by age (1-7 days) and has a representative critical shear stress. As the bed ages, the layers are moved down and the critical shear stress of the layer increases. While this approach can model variations in erodibility with depth, the age layers have typically been too thick (centimeters) to capture the large gradients in τ_{cr} near the upper few millimeters of the bed surface. Additionally, difficulties arise when assigning an age to a bed layer undergoing multiple cycles of resuspension and deposition. By directly tracking τ_{cr} in each bed layer as done by Sanford (2008), the initial conditions of

the model and its algorithms can more directly incorporate site specific data and include the processes of consolidation and swelling.

Sherwood et al. (2007) recently implemented Sanford's (2008) approach within a three-dimensional modeling framework. This paper builds on their efforts by evaluating model behavior within a tidally dominated setting. While consideration of mixed sediment beds that contain both sand and mud is important, this paper focuses on examining the behavior of purely cohesive sediments. The model implementation is verified by comparing results against laboratory erosion experiments conducted using field-collected sediment cores. The sensitivity of erosion to observed seasonal changes in sediment erodibility is examined. Additionally, this paper explores the importance of the consolidation time scale within the context of tidal spring-neap variations in bed shear stresses.

2.3 Methods

To investigate how consolidation influences erosion and deposition in a tidal setting, a cohesive bed model based on Sanford (2008) was implemented that allows τ_{cr} to vary with depth into the bed and simulates consolidation. The model used was a variant of that developed by and described in Sherwood et al. (2007). The vertical profile of bed critical shear stress, $\tau_{cr}(z)$, evolves in time in response to erosion, deposition, consolidation and swelling. Erosion of surface sediment exposes underlying layers of sediment with higher critical stress. Newly deposited sediment has an initially low critical stress that increases with time. Consolidation and swelling are simulated by relaxing $\tau_{cr}(z)$ toward an equilibrium profile $\tau_{ceq}(z)$ (Figure 2.1).

The model was implemented in the Community Sediment Transport Modeling System (CSTMS), an open-source, community developed model integrated within the Regional Ocean Modeling System (ROMS). ROMS is a community developed

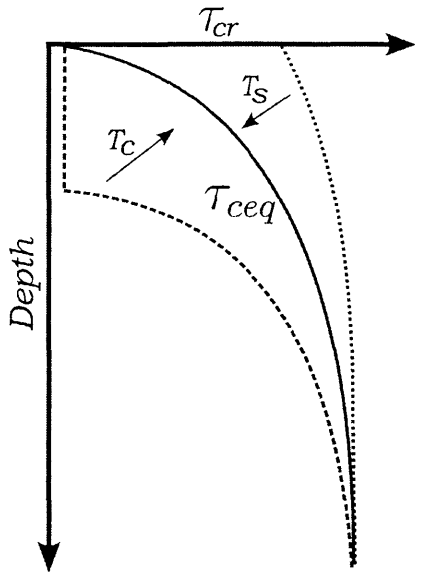

Figure 2.1: Conceptual diagram of consolidation and swelling. The equilibrium critical stress profile $\tau_{ceq}(z)$ is shown as the solid line. The dotted line represents a critical shear stress profile following sediment erosion. The dashed line is a profile after deposition of sediment with a low τ_{cr} at the surface. The arrows indicate consolidation and swelling toward the equilibrium profile with the time scales T_c and T_s respectively. (See Eq. 2.6 in text)

hydrodynamic model written in Fortran 90 and solves the Reynolds-averaged Navier-Stokes equations under the hydrostatic and Boussinesq approximations using a finite-difference, split-mode solver for barotropic and baroclinic modes (Haidvogel and Beckmann, 1999; Shchepetkin and McWilliams, 2005). It uses a curvilinear, Arakawa-C grid with terrain-following s-coordinates. The modular framework allows users to activate and deactivate various advection schemes, turbulence closures, cohesive and non-cohesive sediment transport submodels, and seabed and biology submodels.

As described in Warner et al. (2008), the sediment bed model of the CSTMS divides the seabed into a user-defined number of vertical layers. The fraction and mass of each sediment class as well as bulk bed properties such as porosity, layer thickness, and age, are tracked within each vertical layer in a three-dimensional array. Bed surface parameters like active layer thickness and size-class weighted

mean grain size, mean settling velocity, and mean grain density are maintained in a two-dimensional array for use with bottom boundary layer models. Both the bed and bed surface properties evolve with time to track changes to the seabed.

The CSTMS bed model was modified to account for depth and temporal variability in critical stress in purely cohesive beds by adding an array to track τ_{cr} (Sherwood et al., 2007). Values of τ_{cr} were applied at the top of each bed layer, and critical shear stress was then assumed to vary linearly within a layer. Erosion calculations for all sediment classes were performed using the bed τ_{cr} following Eq. 2.1.

Deposition D was determined by the sediment flux to the bed

$$D = w_s C \tag{2.4}$$

where C is the near-bed concentration and w_s is the settling velocity. No critical stress for deposition was specified. Net erosion or deposition was determined by $N = E - D$ and the sediment was added to the lowest water column cell in the case of net erosion or the top bed cell for net deposition.

If net deposition occurs and the top seabed layer was greater than a user-defined thickness $\delta_{newlayer}$, sediment was removed from the uppermost bed layer by either adding it to the second layer or splitting the top bed layer. Sediment removed from the top layer was added to the second layer if the second bed layer was smaller than a user-defined minimum thickness $\delta_{minlayer}$. The minimum layer restriction was applied to maintain millimeter-scale resolution of the sediment bed near the surface. If the second layer thickness exceeded the minimum layer thickness, the top bed layer was split into a new bed layer of thickness $\delta_{newlayer}$ below the surface layer, with the excess sediment remaining in the top layer. The bottom two layers were then combined to maintain a constant number of sediment layers and conserve sediment mass, consistent with Warner et al. (2008). Deposited sediment was assumed to

have a low critical shear stress $\tau_{cr,min}$. After net deposition, the value of τ_{cr} in the uppermost bed layer was updated as the mean of the previous top layer τ_{cr} and $\tau_{cr,min}$ weighted by the previous layer mass and the newly deposited mass, respectively.

When net erosion occurred, sediment from lower layers was added to the surface layer so that the surface layer thickness remained equal to the active layer thickness. When this resulted in a sediment layer being completely depleted of sediment, the bottom bed layer was split to maintain a constant number of layers. For this model, the active layer thickness was defined as δ_{active} such that $\tau_{cr}(\delta_{active}) = \tau_b$, that is, the thickness at which the bottom stress equaled the bed critical stress. Thus defined, the active layer was usually a few tenths of millimeters thick. After net erosion, the new value of τ_{cr} at the surface was determined by a linear interpolation between the top two bed layers, based on the ratio of mass eroded to the total mass of the layer before erosion.

In order to model consolidation and swelling, the instantaneous critical stress profile is nudged toward an empirically derived reference profile $\tau_{ceq}(m)$ where m is the mass of sediment above a particular bed level (Sanford, 2008). The reference profile takes the form

$$\tau_{ceq}(m) = am^b \tag{2.5}$$

with a and b being empirically derived parameters. This reference profile can be determined by consolidation tests or erosion experiments. The reference equation was formulated in terms of a mass-depth m instead of an actual depth z so that it is unaffected by changes in porosity that alter bed thickness. The mass-depth also allows straightforward application of results from erosion experiments where total eroded mass was measured but porosity may be unknown. Bed layer thickness and mass are related by Eq. 2.3. The model can be formulated using either z or m coordinates because the CSTMS keeps track of both bed layer mass and bed layer

thickness.

The relaxation process was accomplished by updating $\tau_{cr}(m)$ according to a nudging equation:

$$\frac{\partial \tau_{cr}}{\partial t} = \begin{cases} \frac{1}{T_c}(\tau_{ceq} - \tau_{cr}) & \tau_{cr} < \tau_{ceq} \\ 0 & \tau_{cr} = \tau_{ceq} \\ -\frac{1}{T_s}(\tau_{ceq} - \tau_{cr}) & \tau_{cr} > \tau_{ceq} \end{cases} \tag{2.6}$$

where τ_{cr} is the current value of critical stress, τ_{ceq} is the equilibrium value, T_c is the consolidation time scale, and T_s is the swelling time scale (Sanford, 2008). The dependence of both τ_{cr} and τ_{ceq} on mass-depth, m, has been omitted from equation 2.6 for readability, but the equation was applied at each bed level. Equation 2.6 allows for both consolidation after deposition during which τ_{cr} increases and swelling after erosion where τ_{cr} decreases. Typical consolidation time scales T_c are of the order of 1 day while swelling time scales T_s are on the order of 100 days. (Sanford, 2008). In the model, the relaxation step was calculated after the erosion or deposition step and the subsequent updating of bed layers.

2.4 Study site

The model was used to represent conditions in the York River, Virginia, a subestuary of the Chesapeake Bay (Figure 2.2). The York River is a partially-mixed microtidal estuary with a typical tidal range of 0.7 m at the mouth and 1 m at the head (Schaffner et al., 2001). It forms at the confluence of the Mattaponi and the Pamunkey Rivers at West Point, Virginia. Between West Point and Gloucester Point, Virginia, ~40 km, the estuary is straight and consists of a $5 - 10$ m deep channel with 2 m deep shoals on either side. Typical tidal velocities in this region are on the order of $1\,\mathrm{m\,s^{-1}}$ at the surface and $0.4\,\mathrm{m\,s^{-1}}$ at 1 m above the bed (Fugate and Friedrichs, 2003; Kniskern and Kuehl, 2003). Fugate and Friedrichs (2003) reported suspended sediment concentrations at Clay Bank ranging between $50 - 300\,\mathrm{mg\,L^{-1}}$

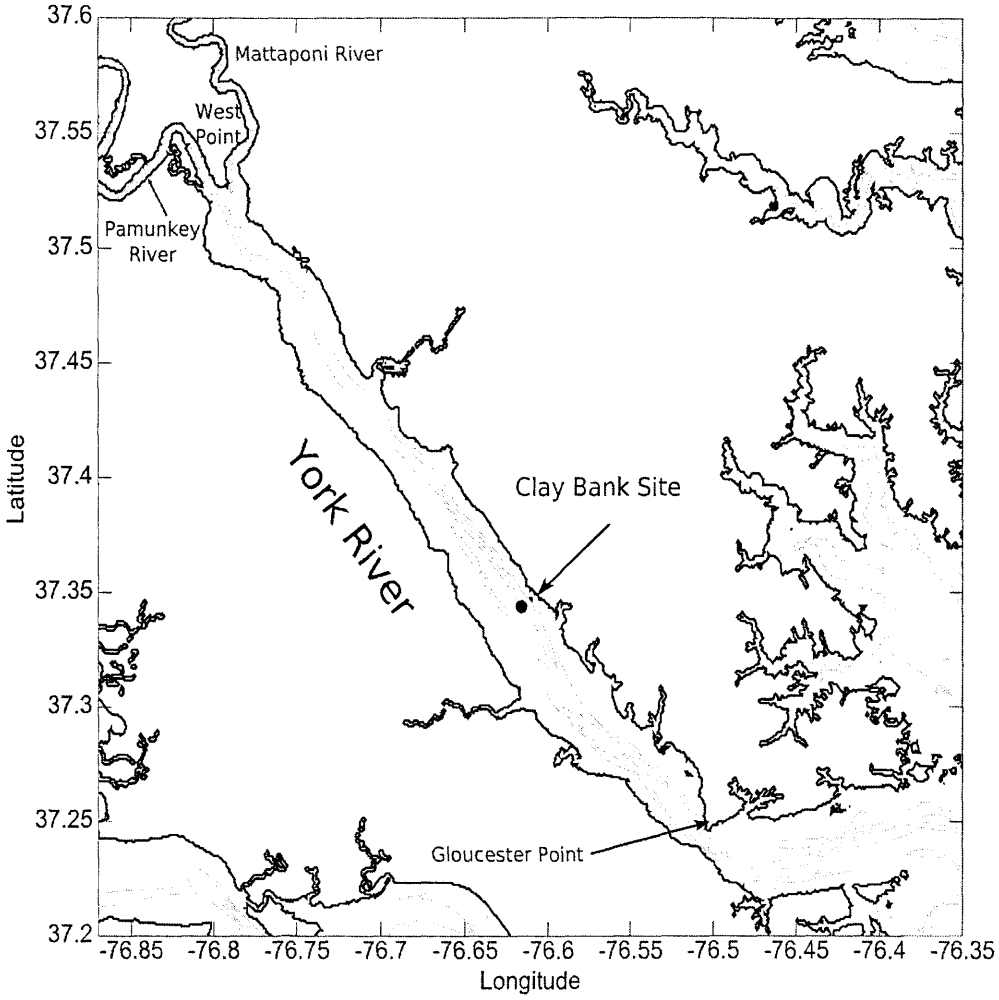

Figure 2.2: The York River, Southeastern Virginia, USA. The Chesapeake Bay lies to the east of the map. The Clay Bank study site is marked. Bathymetric contours drawn every 5 m.

near the bottom and about 20 mg L^{-1} near the surface. Physical disturbance due to repeated tidal erosion and deposition, along with limited consolidation times, likely influence critical stresses of the bed in this region. Due to strong tidal currents, a high range of salinities, and the ephemeral presence of an estuarine turbidity maximum in the upper river (Lin and Kuo, 2001), the influence of benthic biology is likely limited (Schaffner et al., 2001).

Monthly erodibility experiments were conducted at the Clay Bank Channel site (Figure 2.2) in 7.5 m water depth (see Dickhudt et al., in prep.). Two replicate sediment cores were extracted and analyzed using the Gust Microcosm (Gust and Muller, 1997; Thomsen and Gust, 2000). This device used a rotating disc with central suction to apply a known shear stress to a field-collected sediment core sample. Eight steps of increasing stress were applied causing sediment to erode from the core. A flow-through system removes sediment-laden water from the device and through a turbidimeter, generating a time-series of erosion rate vs. applied shear stress. The data were analyzed following the method of Sanford and Maa (2001) (see also Sanford, 2006) and a profile of τ_{cr} and the erosion rate parameter M with mass depth into the bed was determined (Dickhudt et al., in prep.).

The frequent sampling of sediment cores provided data on seasonal variations in erodibility that may have resulted from physical processes like sediment convergence or seasonal changes in biological activity and abundance (Dickhudt et al., in prep.). Data from the Clay Bank site showed a strong seasonal influence, with the site being highly erodible in April, 2006 and least erodible in September, 2006. These data were well suited for specification of erodibility parameters in the model because they provide long-term field measurements of depth variability in τ_{cr} and M.

2.5 Gust Microcosm Simulations

Four one-dimensional model runs simulating the Gust Microcosm experiments were completed to evaluate model performance. The model grid was configured with 8 vertical water column grid cells and 5 x 5 horizontal grid cells to ensure periodic boundary conditions for a one-dimensional simulation within a three-dimensional model. Periodic boundary conditions were enforced at all boundaries so that the model was essentially one-dimensional in the vertical. As bottom boundary stresses cannot be directly forced in the ROMS framework, and the periodic boundary conditions prevent forcing by currents at the boundaries, an alternative method was developed to generate the appropriate bed stresses. A simple wave-bottom boundary layer model was used by specifying wave bottom orbital velocities u_b. Bed shear stress can be determined using $\tau_b = 0.5 f_w u_b^2$ where f_w is the wave-friction factor, set here to 0.3. Appropriate values of u_b were chosen so that the resulting shear stresses were equivalent to the applied shear stresses from the Gust Microcosm experiments.

The bed was initialized with 20 total layers: nineteen 0.2 mm thick layers and a bottommost layer 1 mm thick to prevent total depletion of sediment from the bed. A single sediment size-class was used with a low settling velocity of $w_s = 1 \times 10^{-6}\,\mathrm{mm\,s^{-1}}$. This low settling velocity prevented sediment from redepositing to approximate the removal of sediment from the Gust Microcosm. The sediment grain density was set at $2650\,\mathrm{kg\,m^{-3}}$ and the porosity was kept constant at 0.9 so that the mass of each bed layer was initially $0.053\,\mathrm{kg\,m^{-2}}$.

Both the equilibrium and initial critical stress profiles were initialized using data from the erosion chamber experiments (Figure 2.3a). Two sets of experiments, from April and September, 2006, were used because they represented a highly erodible and a moderately erodible seabed, respectively (Dickhudt et al., in prep.). The simulation was performed for each of the two replicates from each month. Observations

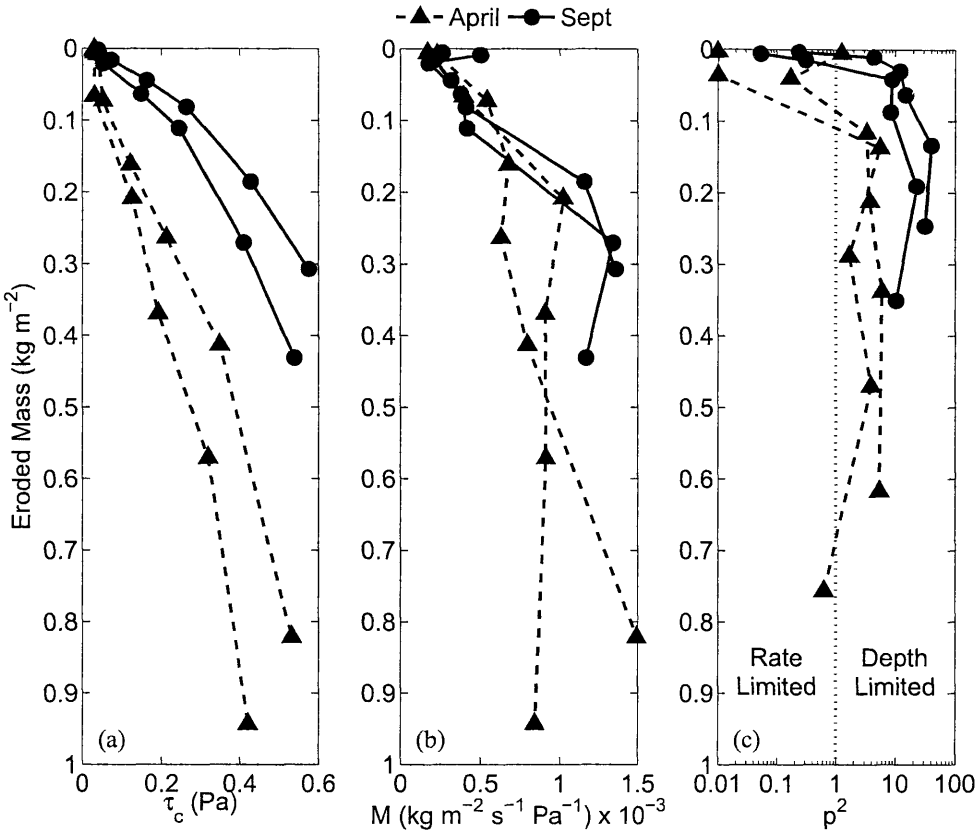

Figure 2.3: Profiles of (a) critical stress and (b) erosion rate parameter determined by the Gust Microcosm experiments. Sediment cores were collected from the Clay Bank site (see Fig. 2.2) in April and September, 2006. Data from Dickhudt et al. (2008) for each of two replicate cores is shown for each month. (c) Erosion type parameter p^2 (Eq. 2.2). Erosion is depth limited when $p^2 \gg 1$ while $p^2 \ll 1$ indicates erosion is rate-limited (Type II).

of M (Figure 2.3b) show some variability over the profile and a general increase with depth. To simplify modeling and to focus on how τ_{cr} controls erodibility, M was held constant with depth within the model. Constant values of M were determined by using the mass-weighted mean of the depth dependent erosion rate parameters determined from the experiments and were $M = 0.8 \times 10^{-3}\,\mathrm{kg\,m^{-2}\,s^{-1}\,Pa^{-1}}$ for April 2006 and $M = 1.1 \times 10^{-3}\,\mathrm{kg\,m^{-2}\,s^{-1}\,Pa^{-1}}$ for September 2006.

The choice of constant M can be further justified by considering values of the erosion type parameter p^2 (Eq. 2.2). Using $\omega = 1.45 \times 10^{-4}\,\mathrm{s^{-1}}$, the tidal semidiurnal radian frequency, values of p^2 where calculated from the profiles of M and τ_{cr} (Figure 2.3c). Except for a thin layer near the surface and the lowermost data point of a single core, depth limitation controls erosion by a factor of 2-40 compared to rate limitation. This analysis shows that, for the Clay Bank site, depth variations in critical stress played a more significant role in determining erosion rate than variations in M for both the spring and fall experiments. In this case, almost all of the eroded sediment column was subject to strongly depth-limited erosion because of high gradients in critical stress. Thus, the precise rate of erosion expressed through the erosion rate parameter M was less important than the fact that erodible sediment was quickly depleted at each stress level.

Results from the Gust Microcosm simulations show that the model predicts the time history of eroded mass well (Figure 2.4). When the applied stress was increased at each step, cumulative eroded mass first rose quickly and then increased slowly as erosion exposed sediment layers having higher critical stress. The greatest model deviations from the observed values were $0.07\,\mathrm{kg\,m^{-2}}$. This corresponds to a difference in sediment concentrations of $9\,\mathrm{mg\,L^{-1}}$ if distributed throughout a 7.5 m water column. Errors between the measured and modeled eroded mass are due to two factors: errors resulting from fitting observed erosion rates to Eq. 2.1 to determine values of M and τ_{cr} and errors resulting from the use of a constant

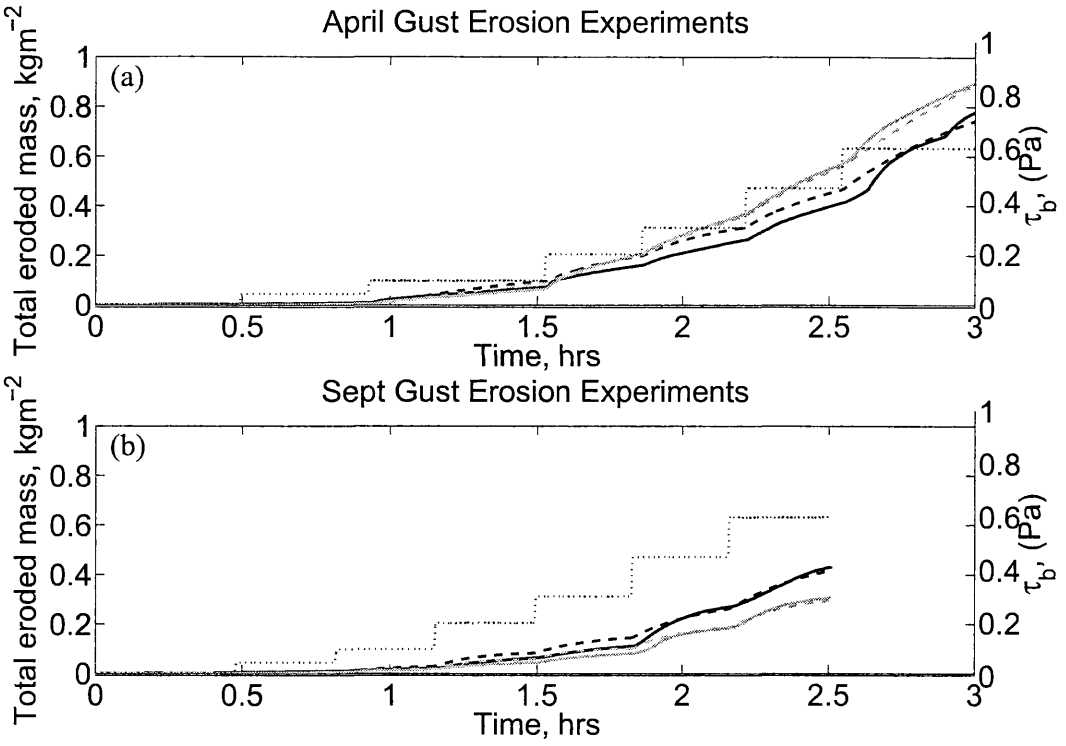

Figure 2.4: Comparison between model estimates to time series from Gust Microcosm experiments for sediment cores collected in (a) April and (b) September, 2006. Solid lines represent cumulative eroded mass during the experiment while dashed lines show the model results (*left axis*). The dotted lines are the applied bed stress (*right axis*). Dark and light lines represent replicate cores from each experiment. Observed values from Dickhudt et al. (2008).

M. The mean difference, averaged over time and all experiments was $0.02\,\mathrm{kg\,m^{-2}}$. This exercise demonstrates that using a constant erosion parameter while preserving depth variations in τ_{cr} captures the erosive behavior seen in the Gust Microcosm experiments.

2.6 Seasonal variations in erodibility

A second set of model runs evaluated the dependence of eroded mass on variations in the initial $\tau_{cr}(z)$ profile under typical spring-neap tidal forcing in an estuary. The replicate cores from September and April were averaged to obtain a single profile of critical stress for each month. Equilibrium profiles were set using a power law fit to the data of both replicates from each month (Figure 2.5). The critical stress of newly deposited material $\tau_{cr,min}$ was set as 0.1 Pa. The thickness at which to create a new bed layer $\delta_{newlayer}$ was set to 0.2 mm and the thickness of the initial bed layers and $\delta_{minlayer}$ was set to 0.1 mm to maintain bed resolution. Water depth was 7.5 m, the depth of the Clay Bank site.

Tidal currents in estuaries are driven by the barotropic pressure gradient that results from changes in free-surface elevation at the estuary mouth. Periodic boundary conditions were necessary to accurately preserve the one-dimensional nature of the model within the three-dimensional ROMS, however, preventing the direct forcing of free-surface elevation at one end of the model domain. ROMS allows prescribed surface stresses to be applied as a body force throughout a user-defined portion of the water column. This capability was used to force a tidally varying barotropic pressure gradient uniformly throughout the water column. Model forcing of the pressure gradient force varied as:

$$\left[\mathrm{a}_0 + \mathrm{a}_1 \cos\frac{2\pi}{14\ \mathrm{days}}\right] \sin\frac{2\pi}{12\ \mathrm{hours}} \tag{2.7}$$

where a_0 is the mean amplitude and a_1 is the amplitude of the fortnightly tidal

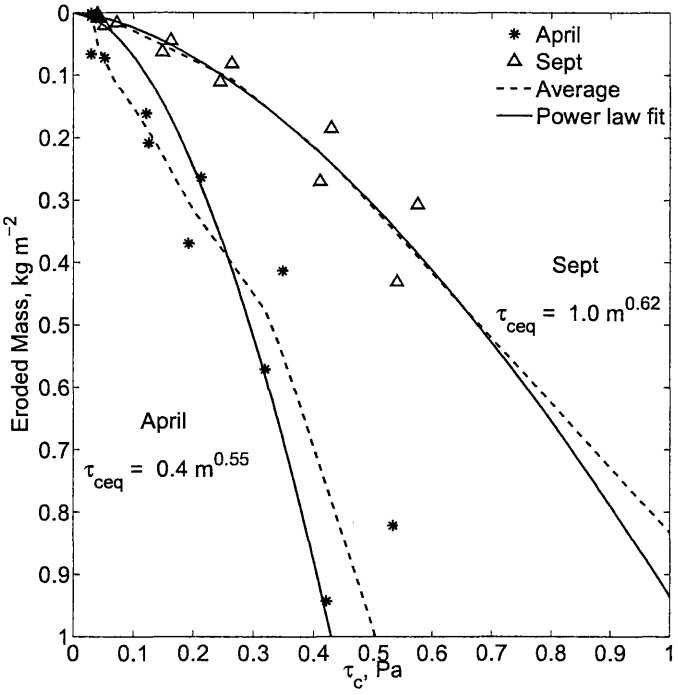

Figure 2.5: Average (dashed lines) and equilibrium (solid lines) critical stress profiles for April and September 2007. Equilibrium profiles obtained by a power-law fit (Eq. 2.5) to the observed values. Symbols show observed data from Dickhudt et al. (2008) (see Fig. 2.3a).

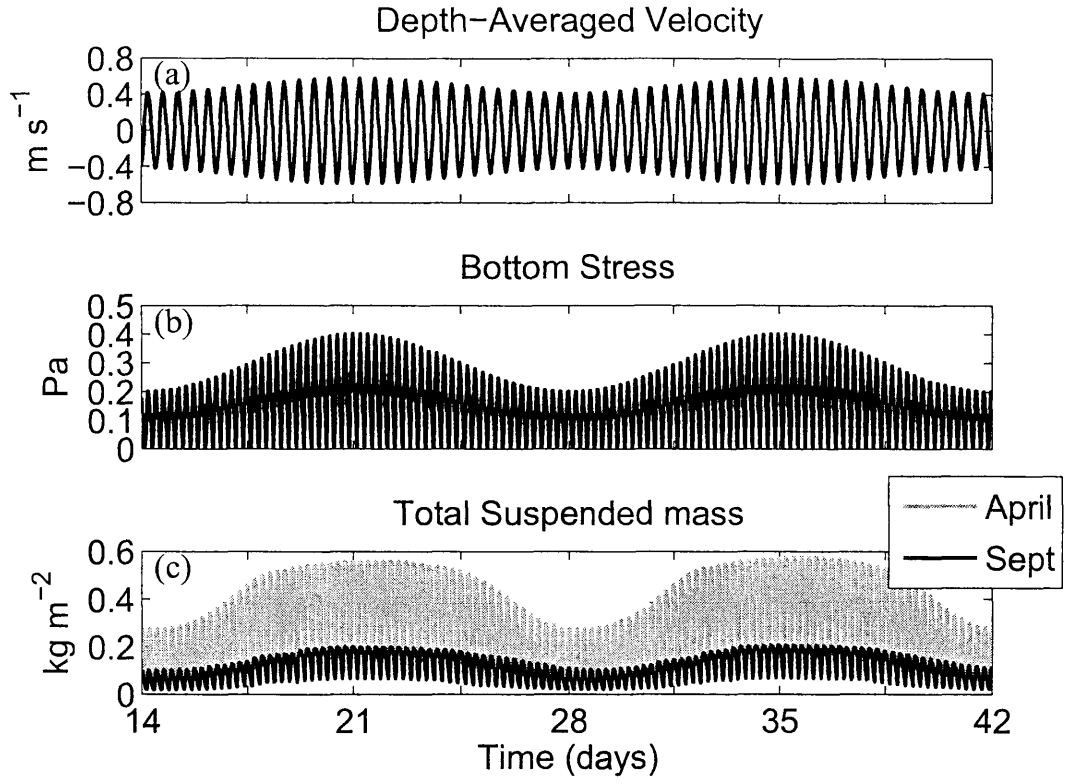

Figure 2.6: Modeled seasonal variations in erodibility over tidal fortnightly time scales for days 14-42. (a) Depth-averaged velocity, (b) bed stress magnitude, and (c) total suspended mass (*bottom*) calculated using April and September critical stress profiles.

variation. The constants a_0 and a_1 in Eq. 2.7 were chosen such that maximum bed stress would range between 0.2 Pa during neap tide to 0.4 Pa during spring tide which are typical values observed in the York River. The model was run for 60 days to allow ample spin-up and show complete spring and neap cycles.

Model results from days 14-42 are presented in Figure 2.6. Depth-averaged velocity and bed shear stress values show typical tidal variability at both semi-diurnal and fortnightly frequencies. For the September simulations, maximum suspended mass during spring tides is $0.2\,\mathrm{kg\,m^{-2}}$ while the neap tide maximum is $0.1\,\mathrm{kg\,m^{-}}2$. The more erodibile April simulations show a larger variation between neap and spring tides with a spring tide maximum of $0.55\,\mathrm{kg\,m^{-2}}$ and a neap tide maximum

of $0.3\,\mathrm{kg\,m^{-2}}$. Additionally, there is a slight asymmetry between maximum eroded mass and maximum tidal stresses. Eroded mass on the decreasing side of the fortnightly cycle, during, for example, days 22 – 25, is slightly greater than on the increasing side due to a consolidation lag in the seabed (Figure 2.6). Sediment deposited immediately following spring tide has a lower critical stress and is resuspended more easily until it has had time to consolidate as also noted by Sanford (2008).

These calculations indicate that seasonal variations in erodibility observed for the Clay Bank site can influence resuspended sediment mass by a factor of 2-3. The model appears capable of representing the effects of spatially and temporally varying cohesive sediment erodibility in a tidally dominated system.

2.7 Sensitivity to consolidation time scale

The model sensitivity to the consolidation time scale was evaluated by repeating the calculations from Section 2.6 using several different values of T_c. For these tests, the initial τ_{cr} profile was assumed to be highly erodible, while the equilibrium profile was less so. This allowed a model test of the consolidation process, representing the evolution of a highly erodible bed toward a less erodible, steady-state configuration. The bed was initialized using the April data from the Clay Bank site, which was observed to be one of the more highly erodibile sediment beds (Dickhudt et al., in prep.). In the absence of consolidation experiments, a power law fit to the September profile was chosen to represent τ_{ceq} (See Figure 2.5). This fit matched the data well ($r^2 = 0.93$) and the September sediment cores were the least erodible of all monthly observations over the 1.5 year period (Dickhudt et al., in prep.). Five simulations were run with consolidation time scales of $T_c = 1$, 6, 12, 24, and 48 hours. This range brackets the value of one day cited by Sanford (2008). Inclusion of an unrealistically

fast consolidation time scale of one hour also provides an example that essentially assumes that sediment bed erodibility remains in the consolidated, equilibrium state regardless of depositional and erosional history.

Figure 2.7 shows the maximum bed stresses and maximum total suspended masses per tidal cycle calculated using each value of T_c. As the consolidation time scale increases from 1 through 12 hours, asymmetry between the neap-to-spring and spring-to-neap transitions becomes more apparent. Longer time scales slow consolidation and allow more sediment to be eroded on the decreasing side of the fortnightly cycle. Additionally, there is a greater difference between spring and neap eroded masses when shorter consolidation time scales are assumed. For $T_c = 1$ hour, the spring-neap difference is about $0.2\,\mathrm{kg\,m^{-2}}$ while for $T_c = 24$ hours the spring-neap difference is only $0.1\,\mathrm{kg\,m^{-}}2$. This is because fast consolidation times result in greater sensitivity to differences in applied shear stress.

The consolidation time scale seems to affect sediment concentrations greatest during neap tides when the difference between eroded mass calculated for $T_c = 1$ hour and $T_c = 48$ hours is about a factor of 2.5. This was similar to the magnitude of differences seen in sediment resuspension estimated to arise from seasonal variation in erodibility. Comparing the estimates that assumed $T_c = 1$ hour to $T_c = 1$ day provided an estimate of the potential cost in assuming an equilibrium τ_c profile. This led to differences in estimated maximum suspended mass that differed by as much as a factor of two. Likewise, uncertainty in the consolidation time scale ($T_c = 12$ to 48 hours) also led to about a factor of two uncertainty in estimates of maximum suspended mass, with differences being highest during neap tides.

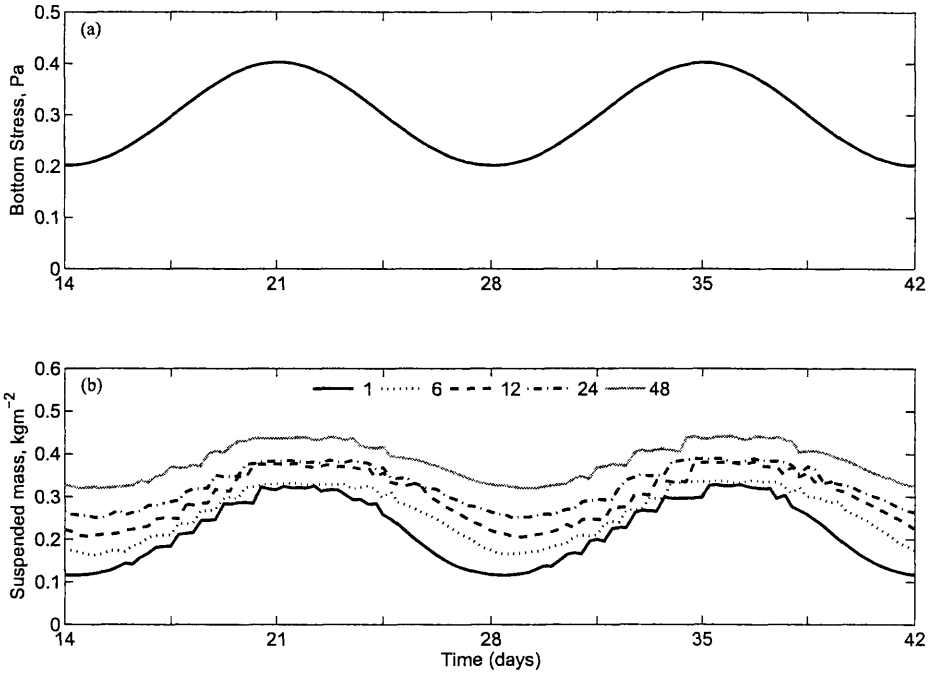

Figure 2.7: (a) Maximum bottom stress and (b) maximum total suspended sediment mass over a tidal cycle for varying values of T_c. Maximum suspended mass estimated assuming consolidation rates ranging from T_c=1 to 48 hours (see legend). Values in (a) and (b) represent the maximum estimated for each tidal cycle.

2.8 Discussion

One parameter typically considered when modeling consolidation is sediment porosity. While porosity exhibits a control on bed critical stress, obtaining high-resolution porosity measurements is difficult, particularly in the upper 1 cm of the sediment bed where critical stress gradients are the greatest. Additionally, observations show very little correlation between sediment porosity and τ_b or M (Dickhudt et al., in prep.). This is most likely due to the effects of biology outweighing differences in porosity between the two seasons at the York River study sites (Dickhudt, pers. comm.). The original Sanford (2008) model included porosity variations and the effects of porosity on M. These processes were not included in the present study, however, both because field data were inconclusive and to simplify the model. For some applications, however, time and depth variations in porosity and M might be important, especially at higher bed stresses when rate limited (Type II) erosion dominates. Future work may incorporate these processes into the CSTMS model.

The linear erosion formulation (Eq. 2.1) was used for two primary reasons. First, the linear formulation requires very little parameterization to accurately model both depth limited and rate limited erosion allowing it to apply over a wide range of hydrodynamic and sediment bed conditions with appropriate observations of τ_{cr} and M (Sanford and Maa, 2001; Piedra-Cueva and Mory, 2001). Additionally, the results from the erosion chamber experiments were analyzed using the same erosion model. Observed values of M and τ_{cr} are difficult to compare under different erosion formulations such that observational and modeling efforts should be standardized.

The Gust Microcosm experiments can only apply shear stresses up to 0.6 Pa which limited this study to examine only relatively small values of τ_b. Erosion devices such as the Sedflume (McNeil et al., 1996) can reach stresses of up to 10 Pa, but cannot resolve millimeter scale variability in the upper seabed. Combining

both Sedflume and Gust Microcosm experiments would provide not only the small scale variability required to accurately resolve tidal conditions, but also the large scale parameters needed to represent more energetic conditions. Combining results from different erosion devices is difficult, however, due to inherent differences in experimental design and the analysis and application of the observations (Sanford, 2006).

Choice of equilibrium profile was an important factor controlling model estimates of eroded mass, especially when consolidation time scales were between 12 and 48 hrs. Extensive monthly sampling of the Clay Bank site provided a large data set to use for model parameterization, but consolidation tests would be useful in determining the appropriate choice of parameters for τ_{ceq} and T_c. A field sampling program that collected multiple cores, used some for initial erosion experiments and reserved others for consolidation testing, could provide data to calibrate all of the important model parameters, namely, the initial τ_{cr} profile, τ_{ceq}, and T_c. In the absence of these data, bed parameters may need to be tuned to fit other observations such as time series of water-column turbidity to validate model estimates in a real world setting.

The model, as presented here, was appropriate for purely cohesive sediment beds. While this approach was acceptable for the muddy Clay Bank site, a more general approach is needed that can be applied to locations that contain both sands and muds. Some models advocate a "threshold" type approach, applying a cohesive bed model if more than some fraction of the bed is mud and otherwise applying a non-cohesive model (van Ledden et al., 2004; Ferre and Sherwood, 2007). This technique, however, may lead to discontinuities in model behavior. A different approach taken by Sanford (2008) used a cohesive erosion formula for the mud fraction of the bed and a non-cohesive formulation for the sands. While this does not allow for the presence of muds and sands to directly influence one another, it may

capture the relevant erodibility behavior and represent consolidation and swelling of muds, as well as bed armoring by sands. Expansion of the model presented here to a mixed grain model is a topic of current research within the CSTMS community (Ferre and Sherwood, 2007).

2.9 Conclusions

A cohesive sediment model following Sanford (2008) that includes depth variations in erodibility and consolidation, has been implemented and tested within the CSTMS (Sherwood et al., 2007). The model tracks the critical stress of each layer and simulates consolidation through a simple relaxation of the instantaneous critical stress profile toward an equilibrium profile. For this paper, model parameters were chosen using observations from erosion experiments performed on sediment cores from the York River, Virginia collected in April and September, 2006 by Dickhudt et al (2008). The model was configured to simulate these experiments and replicated the experimental data using a constant value for the erosion rate parameter (M) and a depth-varying critical shear stress (τ_{cr}). Analysis of the sediment core erodibility data further justified the specification of a constant erosion rate parameter by demonstrating that erosion would be depth limited (Type I) under tidal conditions at Clay Bank.

Additional model runs represented resuspension and deposition under imposed tidal velocities that varied at semidiurnal and fortnightly frequencies. The model estimated that seasonal variations in erodibility accounted for differences in resuspended mass that varied by as much as a factor of 2.5 for the Clay Bank site in the York River. For this location, more sediment would be eroded in the spring (April) than in the fall (September). The greatest differences in suspended mass between the two months occured during neap tides. An asymmetry existed between

the spring-to-neap and the neap-to-spring transitions. More sediment was eroded as tidal maximum bottom stress decreased during the spring-to-neap period due to consolidation lag.

Numerical experiments also tested the sensitivity of calculations to the consolidation time scale, varying T_c from 1 to 48 hours. This yielded differences in estimated eroded mass during neap tide that were of the same order of magnitude as seasonal variations, about a factor of two. Consolidation time scales had the greatest effect on total suspended sediment mass during the spring-to-neap transition. As consolidation time scales grew, this asymmetry increased.

CHAPTER 3

Erodibility and Sediment Trapping in a Partially Mixed Estuary: A Modeling Study of the York River Estuary

3.1 Abstract

Estuarine suspended sediment concentrations are influenced by hydrodynamic forces and sediment and bed properties. Convergence of sediment fluxes and regions of increased erodibility can create estuarine turbidity maxima, local areas of relatively high suspended sediment concentrations. A numerical model of the York River Estuary was developed that included a sediment bed model with time-varying erodibilty and consolidation to examine feedbacks between sediment flux convergence and erodibility. Estimated sediment concentrations and erodibility exhibit high spatial variability in both the along and across channel directions. Model calculations of sediment concentrations and erodibility show similar patterns to observational data. Model results show the development of a highly erodibile pool of sediment near the observed location of the ETM. Even when sediment convergence processes are diminished, suspended sediment concentrations remain high due to high sediment erodibility. Model estimates are shown to be less sensitive to variations in the consolidation rate than in the one-dimensional experiments.

3.2 Introduction

Ubiquitous to estuaries worldwide, estuarine turbidity maxima (ETM) are regions of locally high suspended sediment concentrations near the limit of salt (Dyer, 1995). Schubel (1968) and Postma (1967) proposed that ETM were formed by convergence in near bottom flow landward of the salt limit. Festa and Hansen (1978) represented the gravitational convergence process using a two-dimensional (vertical and along-channel) numerical model. This model is highly sensitive to sediment settling velocity. Sediment with high settling velocities cannot be transported to the turbidity maximum and are deposited upriver. Sediment with low settling velocity are distributed more evenly through the water column, cannot be trapped by gravitational circulation, and escape the turbidity maximum.

The model of Festa and Hansen (1978) produced a turbidity maximum at the salt limit, but the settling velocities used in the study were $0.05\,\mathrm{mms}^{-1}$ to $0.01\,\mathrm{mms}^{-1}$. While these are reasonable values for unfloculated sediment, most estuarine suspended sediment is packaged as aggregated flocs that settle faster ($O(1\,\mathrm{mms}^{-1})$) (Hill and McCave, 2001), indicating that processes other than net gravitational circulation contribute to ETM formation. Using a simple numerical model, Geyer (1993) showed that the suppression of turbulence by density stratification due to salinity near the salt limit can trap twenty times more sediment than net gravitational circulation alone. Suspended sediment becomes trapped in the bottom layer near the head of salt and cannot be entrained into the upper layer due to damping of turbulent mixing by stratification. Tidal asymmetries in vertical velocity and suspended sediment profiles can also produce ETMs, especially in macrotidal systems (Jay and Musiak, 1994). While these processes tend to be most important near the head of salt, they can also create ETMs in other areas where the channel geometry alters the salinity field (Schoellhamer, 2001; Woodruff et al.,

2001; Lin and Kuo, 2001).

In some estuaries, additional turbidity maxima, called secondary turbidity maxima (STM) are observed far from the limit of salt. In the Hudson River Estuary, Geyer et al. (2001) reported a turbidity maximum formed by tidal straining and lateral convergence of sediment in a region where salinities were 12-16 psu. Roberts and Pierce (1976) found an STM near a channel constriction in the Patuxent River Estuary. In the York River, Lin and Kuo (2001) measured an STM approximately 40 km upstream of the river mouth where the water column transitions from well-mixed to partially-stratified due to channel shoaling. A three-dimensional numerical model of the York River was able to reproduce the location of the STM and suggested that its position and magnitude depended on river flow and the spring-neap tidal cycle (Lin and Kuo, 2003). During high flow conditions, only one ETM was present around 40 km upstream of the river mouth, while two ETMs were present during low flow conditions where a transition between stratification regimes existed. While Lin and Kuo (2003) were able to simulate the STM location reasonably well, they also found that resuspended sediment supply from the bed was important in determining the turbidity magnitude.

Estuarine turbidity is controlled by a complex set of factors. Spatial variations in erodibility may be important for ETM dynamics (Wellershaus, 1981; Lang et al., 1989; Friedrichs et al., 1998). Hydrodynamic, seabed, and biological processes can interact, to create feedbacks between water column concentrations and seafloor properties on various scales. While convergence processes influence the location of turbidity maxima, sediment erosion on tidal timescales controls the magnitude of suspended sediment. When sediment supply is limited, the ETM location can decouple from the salt limit and may be located near an erodible bottom deposit (Sanford et al., 2001; Warner et al., 2007). Many existing models fail to account for these feedbacks controlling spatial variation of turbidity and erodibility and for

timescales of bed consolidation that may influence the persistence of an ETM. Using a numerical model of the York River Estuary, this study examined how sediment trapping and erodibility affect estuarine suspended sediment concentrations by incorporating a sediment bed model that includes spatial variations in erodibility and consolidation.

3.3 Study Site

The York River (Figure 3.1) is a partially-mixed microtidal estuary with a typical tidal range of 0.7 m at the mouth and 1 m at the head (Schaffner et al., 2001). It forms at the confluence of the Mattaponi and the Pamunkey Rivers at West Point, Virginia. Between West Point and Gloucester Point, a distance of 40 km, the estuary is straight and consists of a 5-10 m deep channel with 2 m deep shoals on either side. At Gloucester Point, the river turns toward the north, widens from around 3 to 6 km, and the channel depth increases to 20 m with a broad northern shoal and a narrow southern shoal. This configuration divides the river into two regimes: the broad, deep, exposed lower river, where resuspension of sediment is likely driven by waves during storms, and the narrow, shallow upper river dominated by tidal currents (Dellapenna et al., 2003). Benthic biology is less prevalent in the upper river due to the more intense tidal currents, a greater range of salinities, and the ephemeral presence of a secondary turbidity maximum (STM)(Schaffner et al., 2001). Physical processes like erosion and deposition during tidal cycles likely control critical shear stresses of the bed in this region. In constrast, tidal currents in the lower, deeper river are generally less intense and the bed is disturbed only during storms. Because of the less frequent occurrence of bed disturbance, sediment dynamics in the lower river likely reflect biologic control through biostabilization, biodestabilization, and bioturbation.

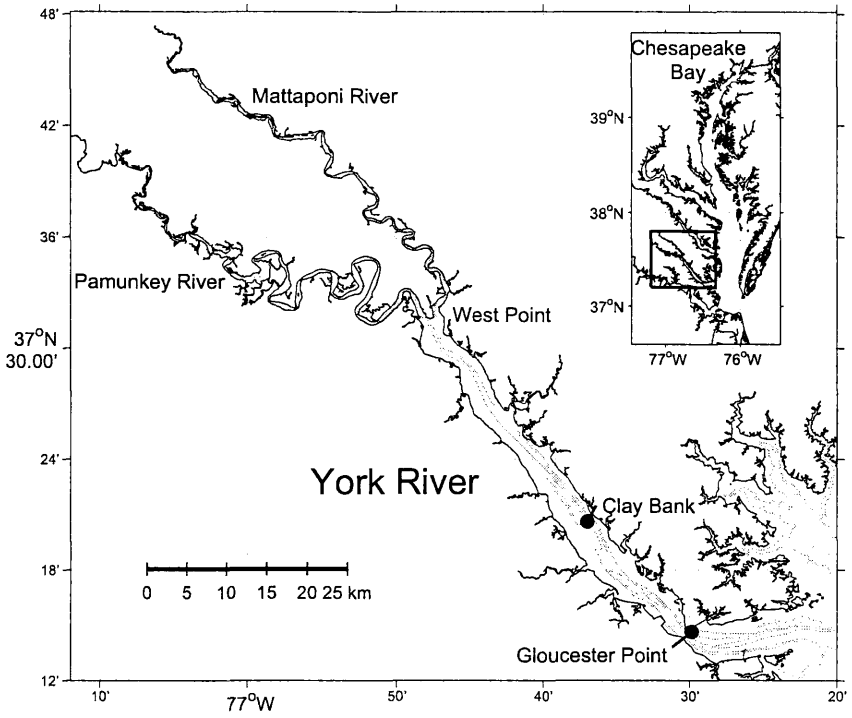

Figure 3.1: York River, Virginia, USA. Light contours are bathymetry in 5 m intervals The study locations at Clay Bank and Gloucester Point are marked. Inset map shows location of the York River within the Chesapeake Bay

The York River has been well studied, particularly near Clay Bank (see Figure 3.1). Typical tidal velocities are on the order of $1\,\mathrm{ms}^{-1}$ at the surface and $0.4\,\mathrm{ms}^{-1}$ at 1 meter above the bed (Fugate and Friedrichs, 2003; Kniskern and Kuehl, 2003). At Clay Bank, Fugate and Friedrichs (2003) reported suspended sediment concentrations ranging between 50 - $300\,\mathrm{mgL}^{-1}$ near the bottom and about $20\,\mathrm{mgL}^{-1}$ near the surface. Also at Clay Bank, Maa and Kim (2002) determined values of bed shear stress during spring tidal conditions to be 0.4-0.9 Pa using a tripod mounted with four Electro-Magnetic Current Meters (EMCM) and a log-layer approach.

Lin and Kuo (2001) observed an STM about 40 km from the mouth in the transition region between a well-mixed and stratified water column. They concluded that the STM was maintained by sediment resuspension and turbulence damping in the transition zone due to salinity stratification. Using the numerical Hydrodynamic Eutrophication Model (HEM-3D)(Park et al., 1995) they were able to simulate the spatial locations of the turbidity maxima, but the magnitude of the simulated results were only $40\,\mathrm{mgL}^{-1}$, a factor of 2.5 lower than the observed concentrations of $100\,\mathrm{mgL}^{-1}$ (Lin and Kuo, 2003). Their model, however, used a constant value of critical shear stress ($\tau_c = 0.1\,\mathrm{Pa}$) and a limited bed sediment supply determined by initializing the bed with deposited sediment thickness of a prior model case. Incorporating a spatially variable but steady erosion rate, Kwon (2005) was able to reduce errors in bottom suspended sediment concentrations by 55%. Without simulating the feedbacks between sediment depostion and erosion, these models may not be able to recreate a pool of highly erodible sediment in the vicinity of the STM.

Results from ^{210}Pb radioisotope studies suggest that physical mixing depths in this region are around 40 to 120 cm while x-radiographs show little evidence of bioturbation, indicating active resuspension and deposition processes over seasonal to decadal timescales (Dellappenna et al., 1998). Further observations revealed century-scale residence times for particles in the physical mixed layer while the

mass of sediment in the layer was equivalent to about 70 years of river sediment yield (Dellapenna et al., 2003).

Recent work by Dickhudt (2008) has shown sediment erodibility to vary in the Clay Bank region over seasonal timescales. During the late winter and spring (February-May), erodibility at Clay Bank is generally greater than during the summer and fall with greatest erodibilities occurring in April and May. At Gloucester Point, however, there was little seasonal variation in erodibility. Dickhudt (2008) argued that increased freshwater during February through May alters trapping processes and creates a region of highly erodible sediment near Clay Bank. These "mud reaches" have been observed in other estuaries including the Hudson (Geyer et al., 2001) and the Weser (Uncles and Stephens, 1989). The presence of a STM in the region during high river flows is consistent with this hypothesis. While insufficient erodibility and water-column data are available to verify this speculation, three dimensional numerical models allow us to examine the processes involved in estuarine sediment trapping and the creation of a mud reach.

3.4 Methods

A three-dimensional representation of the York River Estuary was developed using the Regional Ocean Modeling System (ROMS) v3.1 (Shchepetkin and McWilliams, 2005; Warner et al., 2008; Haidvogel et al., 2008). ROMS solves the hydrostatic Reynolds-averaged Navier-Stokes equations on a curvilinear orthogonal grid with vertical stretched terrain-following coordinates. The modular system allows users the choice of several types of boundary conditions, advection schemes, turbulence parameterizations, and sub-models such as biology and sediment (Warner et al., 2008). For this study, ROMS was configured using the Mellor and Yamada level 2.5 turbulence closure model (Mellor and Yamada, 1982), third-order upstream advection

for momentum and MPDATA advection for tracers (Smolarkiewicz and Margolin, 1998). A sediment model similar to Warner et al. (2008) was included with the bed model (Sanford, 2008) modified to include variations in critical shear stress with depth, and consolidation and swelling processes as presented in Chapter 2.

3.4.1 Cohesive Bed Model

A cohesive sediment bed model, based on Sanford (2008), was implemented in ROMS to represent consolidation processes and the increase of critical shear stress with depth as typically seen in muddy seabeds. Chapter 2 described the model implementation within ROMS, but a brief summary follows. The seabed was represented by a user-defined number of layers. The critical shear stress for erosion $\tau_{cr}(m)$ was specified at the top of each bed layer, with m being the sediment mass above that bed layer. When sediment was eroded, the critical stress at the bed surface increased as layers with higher τ_{cr} became exposed. Sediment deposited to the bed created an easily erodible layer at the bed surface with an assumed low critical stress, $\tau_{cr} = 0.05\,\mathrm{Pa}$.

The model accounts for the effects of consolidation on τ_{cr} using a relaxation equation. The bed sediment was assumed to have an equilibrium critical stress profile $\tau_{ceq}(m)$ that represents the critical stress profile of a fully consolidated bed. The instantaneous profile of $\tau_{cr}(m)$ was adjusted at the end of every model time-step to simulate consolidation and swelling by adjusting the most recent profile $\tau_{cr}(m)$ toward τ_{ceq} according to

$$\frac{\partial \tau_{cr}(m)}{\partial t} = \begin{cases} \frac{1}{T_c}(\tau_{ceq}(m) - \tau_{cr}(m)) & \tau_{cr}(m) < \tau_{ceq}(m) \\ 0 & \tau_{cr}(m) = \tau_{ceq}(m) \\ -\frac{1}{T_s}(\tau_{ceq}(m) - \tau_{cr}(m)) & \tau_{cr}(m) > \tau_{ceq}(m) \end{cases} \tag{3.1}$$

where T_c and T_s are e-folding timescales for consolidation and swelling, respectively. For the following model experiments, $\tau_{ceq}(m) = 1.0m^{0.62}$ which was a power-law fit

of erodibility experiments performed by Dickhudt (2008) on field-collected cores in September 2007 as presented in Chapter 2.

Erosion occured when hydrodynamic bed stresses τ_b exceed τ_{cr} at the sediment surface. Following Sanford and Maa (2001), the erosion rate was determined as E ($\mathrm{kg\,m^{-2}\,s^{-1}\,Pa^{-1}}$), where

$$E = M(\tau_b - \tau_{cr}(z)) \tag{3.2}$$

τ_b is the bed shear stress (Pa), $\tau_{cr}(m)$ is the critical shear stress for erosion (Pa), and M is the erosion rate parameter ($\mathrm{kg\,m^{-2}\,s^{-1}\,Pa^{-1}}$). The original model of Sanford (2008) allowed M to vary with depth as a function of solids volume fraction ϕ_s. Here, however, both solids fraction and the erosion rate parameter were held constant with $\phi_s = 0.1$ and $M = 1 \times 10^{-3}\,\mathrm{kg\,m^{-2}\,s^{-1}\,Pa^{-1}}$, as in Chapter 2. As explored in Chapter 2, erosion in the York River is primarily depth-limited and hence depends more greatly on the critical stress profile than on the erosion rate parameter.

3.4.2 York River Model

Previous modeling studies have been performed for the York River using HEM3D (Lin and Kuo, 2003; Kwon, 2005). The model grid from Kwon (2005) was modified to be compatible with ROMS for this study (Figure 3.2). Average grid resolution was 170 m in the along-channel direction and 110 m in the cross-channel direction. The major tributaries of the York, the Mattaponi and Pamunkey Rivers, were represented in the model with only one cell in the cross-channel direction due to their narrow width. The model extended to the fall line near Hanover, VA on the Mattaponi and Beulahville, VA on the Pamunkey. Stretched terrain following coordinates were used, with 20 grid cells vertically and increased resolution at the seafloor and water surface.

To initialize the model, ROMS was run for 60 days using the 60 year median

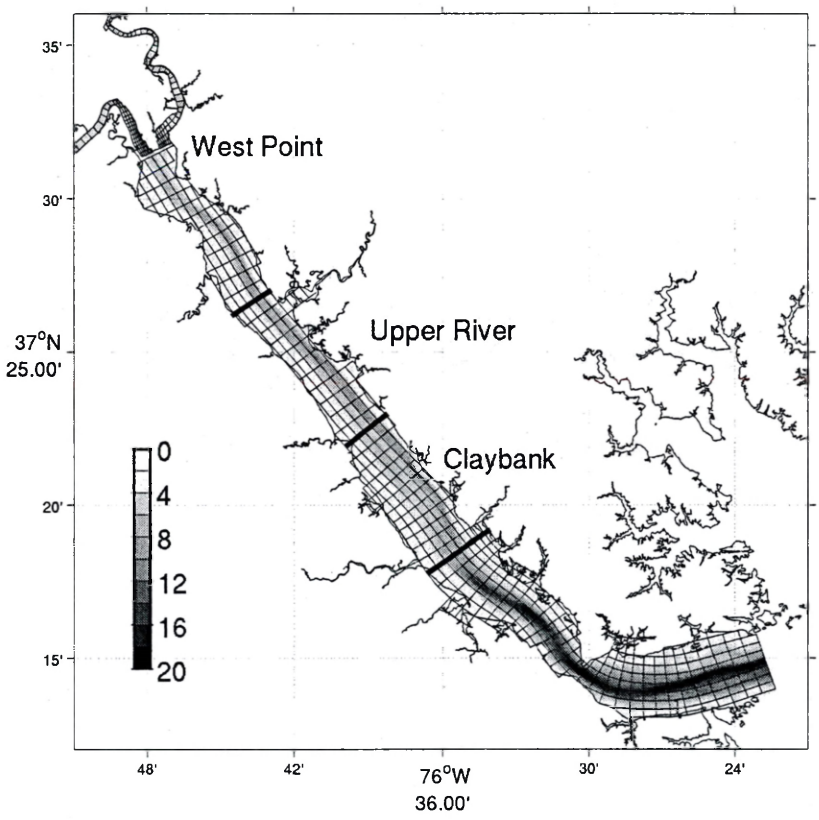

Figure 3.2: York River model grid. Below West Point every 5th grid cell is shown. Above West Point, every grid cell is shown. Dark lines and labels indicate boxes used for sediment flux calculations. (See 3.6.1)

freshwater flow of $42\,m^3s^{-1}$ from the Pamunkey river and $25\,m^3s^{-1}$ from the Mattaponi river and a spring-neap tidal cycle with 0.2 m neap amplitude and 0.4 m spring amplitude. Values obtained from the final time-step of these calculations were used to initialize the velocity and salinity fields.

The sediment bed was initialized in a similar manner using results from the 60 day run. Two cohesive sediment classes were used with settling velocities of $0.8\,mms^{-1}$ and $0.1\,mms^{-}1$. To initialize the 60 day run, they were distributed in equal fractions throughout the model domain with a total bed thickness of 2.9 mm. Bed critical stress was set throughout the river to be constant (0.05 Pa) with depth. Based on the results of Chapter 2, a consolidation timescale of $T_s = 24\,hrs$ and a swelling timescale of $T_s = 2400\,hrs$ were used. The bed was allowed to evolve during the initialization procedure which created areas of high sediment erodibility along the shoals of the estuary and the channel flanks (Figure 3.3). Sediment was removed from the main channel, leaving behind a bed with low erodibility. Bed erodibility and sediment distribution from the end of the 60 day run were used to initialize the longer, more realistic model.

The model was then run to simulate the first 200 days of 2007. At the fall-line, sources of freshwater were specified using data from USGS gages 1674500 near Beulahville, VA for the Mattaponi and 1673000 near Hanover, VA for the Pamunkey. Suspended sediment concentrations of water entering the estuary from upstream were set at $5\,mgL^{-1}$. While a constant value is physically unrealistic, this represents normal suspended sediment concentrations at the boundaries, and sediment from upriver sources generally remains trapped at the primary ETM at West Point and therefore does not influence conditions downstream.

At the open boundary, sea-level was varied according to sea-surface height data from the Coast Guard pier at Yorktown. The available data was lagged by 1 hr and scaled by a factor of 1.4 to account for tidal wave deformation from the river

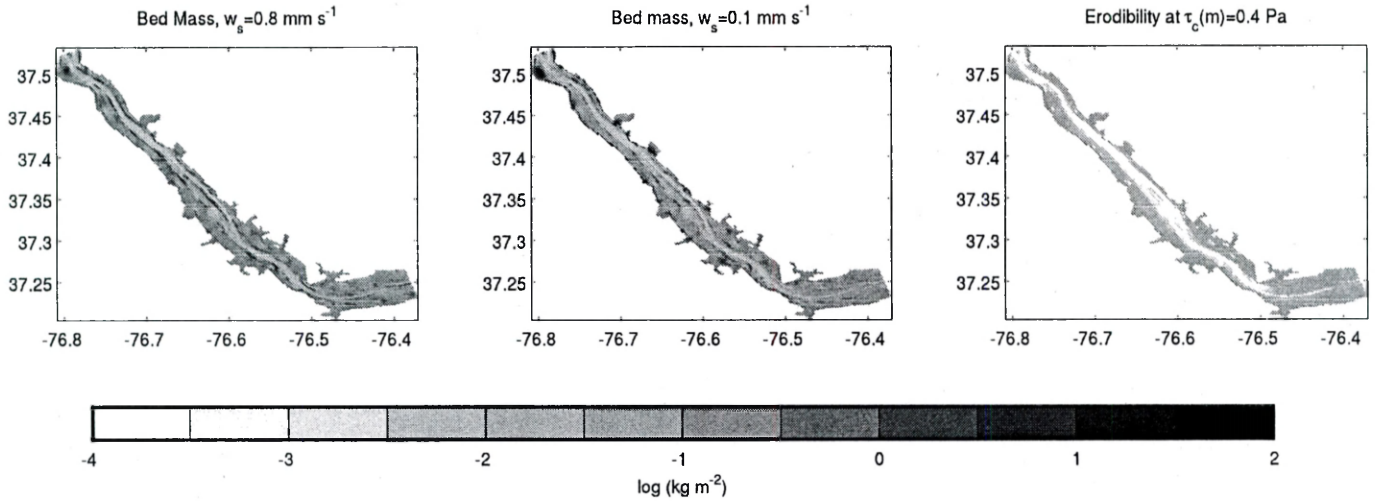

Figure 3.3: Model initial bed conditions estimated after 60 day spring-neap tidal cycle and median river flow (see text for details). (a) Total bed mass of $0.8\,\mathrm{mms}^{-1}$ settling velocity size class. (b) Total bed mass of $0.1\,\mathrm{mms}^{-1}$ settling velocity size class. (c) Total bed mass above $\tau_{cr}(m) = 0.4\,\mathrm{Pa}$. Shading is based on a log scale.

mouth to the Coast Guard pier. These values were chosen so that modeled time series of water elevation at the Coast Guard pier matched the observations. A zero gradient condition was applied for suspended-sediment concentration at the boundary. Open-boundary salinity was specified following Warner et al. (2005) where the salinity gradient at the open-boundary is determined from an empirical relationship. The salinity along the river is assumed to fit the hyperbolic tangent function,

$$\frac{S_0}{2}\left[1+\tanh(2-\frac{X}{\beta})\right] \tag{3.3}$$

where S_0 is the maximum salinity at the ocean or bay end, X is the along-channel distance, and β is a length scale for the salt intrusion, based on river flow. The horizontal gradient at the open boundary can then be specified from the derivative of Eq. 3.3 with respect to X,

$$\frac{\partial s}{\partial x}(1,y,z,t) = -\frac{S_0}{2\beta}\mathrm{sech}^2\left(\tanh^{-1}\left(\frac{2s_1}{S_0}-1\right)\right) \tag{3.4}$$

where s_1 and $\frac{\partial s}{\partial x}(1,y,z,t)$ are the salinity and the salinity gradient at the first interior point. The salinity at the boundary s_0 is then defined as

$$s_0 = s_1 - \frac{\partial s}{\partial x}\Delta x \tag{3.5}$$

where Δx is the along channel grid cell width.

Data from the Chesapeake Bay Program were used to fit β in Eq 3.3. Best fit values of β were then regressed against 4 day mean, 4 day lagged river flow Q_4 resulting in $\beta = 290/Q_4 + 50$. These data fit the hyperbolic tangent function with $r^2 = 0.65$.

3.4.3 Analysis of Results

To investigate temporal variations in suspended sediment and erodibility, time-series of the study sites at Clay Bank and Gloucester Point are presented below.

Model results have been tidally averaged using a 36 hr low-pass filter to examine subtidal sediment transport. Erodibility data is presented as the sediment bed mass above a particular value of τ_{cr}, generally 0.4 Pa. For example, if the critical stress profile at a location matched the equilibrium critical stress profile $\tau_{ceq} = (m) = 1.0m^{0.62}$ the erodibility at 0.4 Pa would be 0.23 $\mathrm{kgm^{-2}}$. Higher erodibility values would be indicative of an unconsolidated bed. Erodibility values below 0.23 $\mathrm{kgm^{-2}}$ indicate that the critical stress profile is more consolidated than the equilibrium profile. Such cases could still have a thin surface layer of relatively unconsolidated sediment above a previous erosional plane such that surface sediment is consolidating while sediment at depth is swelling.

An along-channel transect following the south-western flank of the river channel and an across-channel transect at Clay Bank were chosen to examine sediment transport processes spatially. Two time periods were chosen to represent (1) spring conditions with higher river flows (Day 115, 26 April 2007) and (2) summer conditions with reduced river flow (Day 180, 30 June 2007) to analyze these transects under seasonal variations in forcing. Finally, the model sensitivity to the consolidation timescale was tested because this parameter is particularly poorly constrained and results from Chapter 2 showed particular sensitivity to T_c.

3.5 Results

Time-series of input river flow, along with model estimates of tidal range, bed stress, suspended sediment, and erodibility from Clay Bank and Gloucester Point are presented in Figure 3.4. During the first half of the time-series, when large river pulses occurred, suspended sediment concentrations and erodibility were greatest. As river flow dropped in late spring and early summer, suspended sediment concentrations and erodibility fell. While similar bed stresses occur during these time pe-

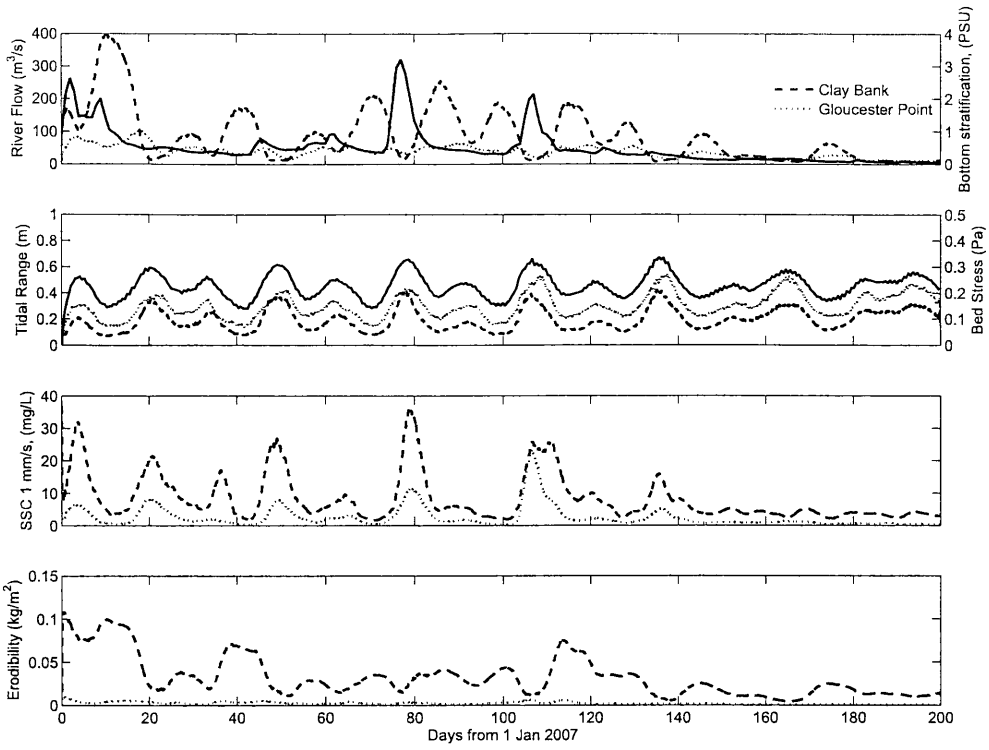

Figure 3.4: Modeled tidally-averaged time-series of sediment and hydrodynamic properties at Clay Bank (dashed) and Gloucester Point (dotted). (a) River flow (left axis,solid line) and salinity difference (right axis) in the lower half of the water column at Gloucester Point and Clay Bank. (b) Tidal range (left axis,solid line) and bed stress (right axis) at each study site. (c) Near-bed (0.5 mab) suspended sediment concentrations at each study site. (d) Sediment erodibility at each site defined as m where $\tau_{cr}(m) = 0.4\,\mathrm{Pa}$. Tidal averaging was accomplished with a 36-hr filter.

riods, erodibility and suspended sediment concentrations decreased indicating that the erodible mass of sediment had moved away from the Clay Bank area or had consolidated.

At Gloucester Point suspended sediment concentrations remain low throughout the modeled period. Even though bed stresses were greater than was estimated for the Clay Bank site, sediment erodibility was low, limiting the amount of sediment available for resuspension. During the spring, sediment erodibility at Clay Bank was much greater than at Gloucester Point. During the summer months, however.

sediment erodibility at both locations was much lower.

Typical along-channel transects of sediment concentration and bed erodibility for a high erodibility period (Day 115, 26 April 2007) are presented in Figure 3.5. This high erodibility period occurred in the wake of a period of high stratification that followed higher river discharge and neap tide. Above 35 km from the river mouth, the water column was stratified and a STM was located near 48 km. Bed erodibility and bed thickness were greatest in the area of the STM indicating deposition of erodible material. The STM was maintained in the region due to a subtidal convergence of sediment flux. The primary ETM was also apparent further upriver, but was not associated with a highly erodible bed.

Later in the model run, when river discharge was low (Day 180, 30 June 2007), the water column was well mixed and suspended sediment concentrations were lower throughout the river (Figure 3.6). An STM was still present near 48 km, but sediment concentrations were lower and the STM was smaller. Erodibility at 1 Pa fell from 3.5 $\mathrm{kg\,m^{-2}}$ to 2 $\mathrm{kg\,m^{-2}}$ while the total bed mass remained nearly constant indicating consolidation of bed sediment since day 115. Residual fluxes reversed direction and convergence lessened indicating that the reduction of sediment trapping mechanisms had relaxed, but that the STM remained due to enhanced erodibilities still present in the region.

3.5.1 Spatial variability of sediment processes

The model estimated significant spatial variability in erodibility and suspended sediment concentrations (Figure 3.7). While suspended sediment concentrations were greatest along the southern shoals of the river and during the spring season, bed shear stresses were highest in the channel. The lack of correlation of shear stress and sediment concentrations indicated that bed sediment supply and sediment convergence controlled the suspended sediment concentrations during both the wet

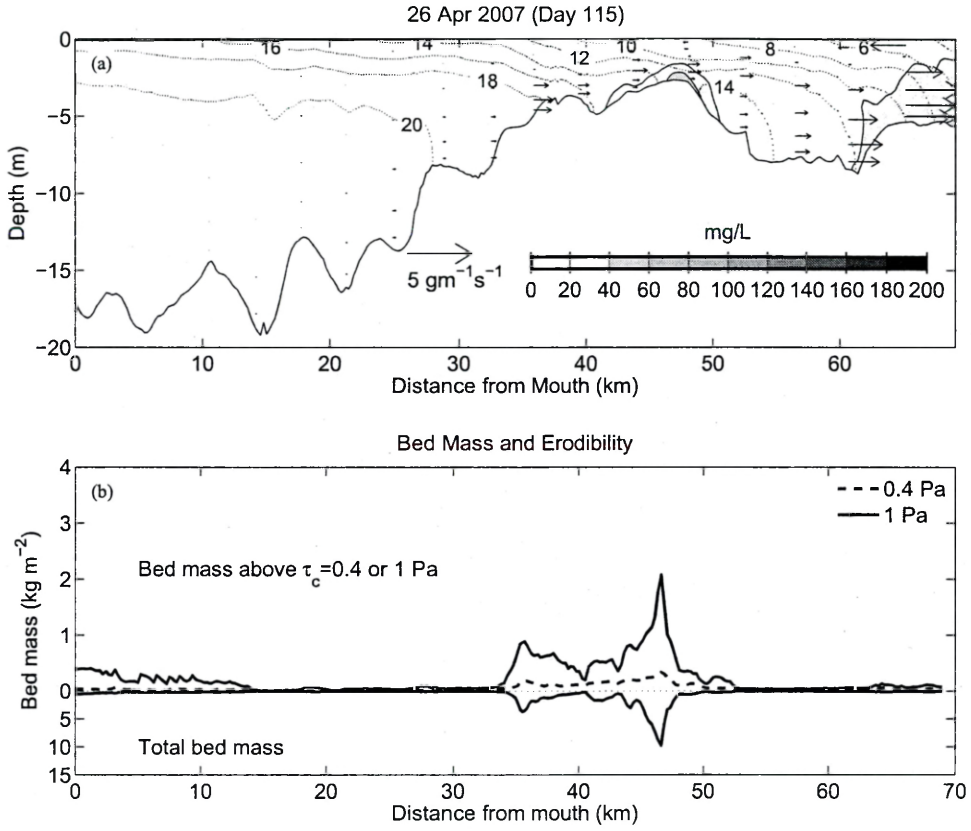

Figure 3.5: Modeled, tidally averaged, along-channel hydrodynamic and sediment properties Day 115 (26 April 2007). (a) (filled contours) Suspended sediment concentrations, (dotted contours) salinity, and (arrows) along-channel sediment flux along the southern channel flank. (b) Sediment erodibility (positive upward) and total bed mass (positive downward)

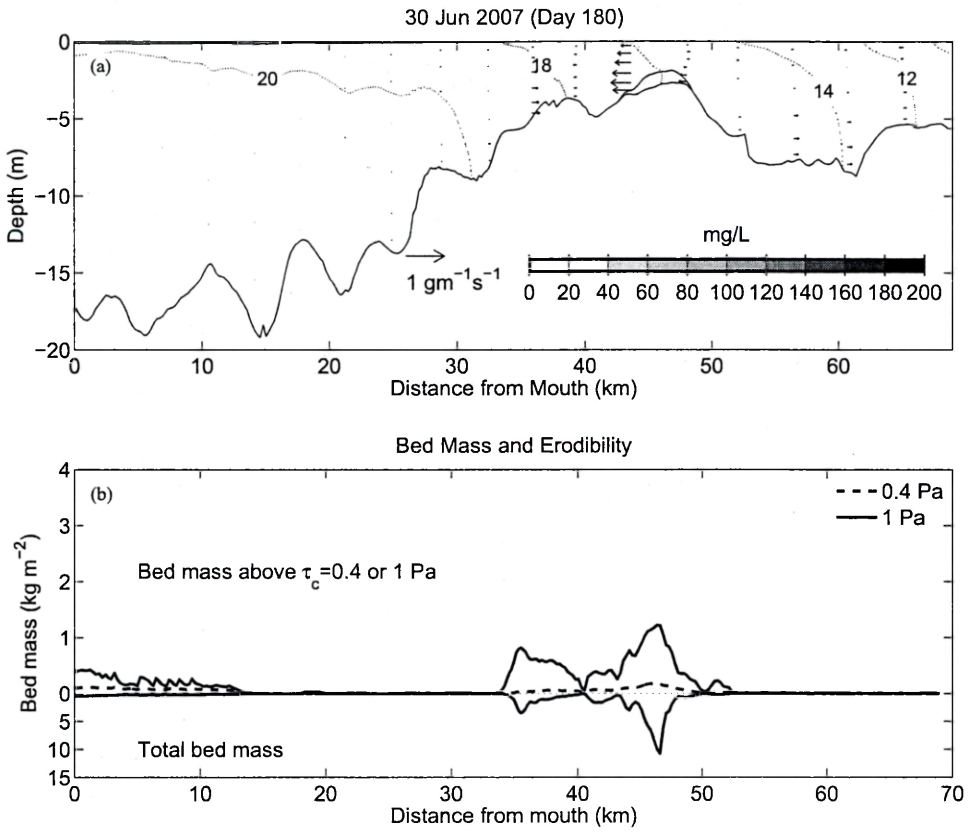

Figure 3.6: Modeled, tidally-averaged, along-channel hydrodynamic and sediment properties Day 180 (30 June 2007). (a) (filled contours) Suspended sediment concentrations, (dotted contours) salinty, and (arrows) along-channel sediment flux along the southern channel flank. (b) Sediment erodibility (positive upward) and total bed mass (positive downward)

(day 115) and dry (day 180) seasons. Additionally, as the spin-up calculations were initialized with a uniform sediment bed, sediment was removed from the main channel and redeposited along the shoals and flanks in areas of lower shear stresses. On day 115, there was one large ETM extending from West Point to Clay Bank. Concentrations were highest on the northern shoals near West Point but further downriver concentrations were highest on the southern shoals.

Bed erodibility generally followed the same pattern as suspended sediment. Erodibility was greatest on the shoals while sediment was scoured from the channels exposing layers of much higher critical bed stress at the sediment surface. Also, near Clay Bank, there were tongues of high erodibility on the channel flanks. Downriver at Gloucester Point, however, high bed erodibility existed even though suspended sediment concentrations were low. This was most likely due to the greater depths and lower bed shear stresses here. Sediment was not scoured from these regions and remained near the equilibrium profile erodibility value of $0.23\,\mathrm{kg\,m^{-2}}$.

To explore the three-dimensional nature of sediment transport in the STM, cross-channel transects of suspended sediment and erodibility were investigated. In April, suspended sediment concentrations were greatest on the channel flank and the western shoals (Figure 3.8). High suspended sediment concentrations there coincided with increased erodibility and bed thickness. Figure 3.9 shows cross-channel results on day 180 (30 June 2007). Suspended sediment concentrations were reduced somewhat compared to day 115 and erodibility was lowered. Sediment trapping was likely caused by the convergence of cross-channel flows.

3.6 Discussion

Along-channel sediment dynamics were evaluated through a simplified box model approach to explore the movement of sediment throughout the estuary. The

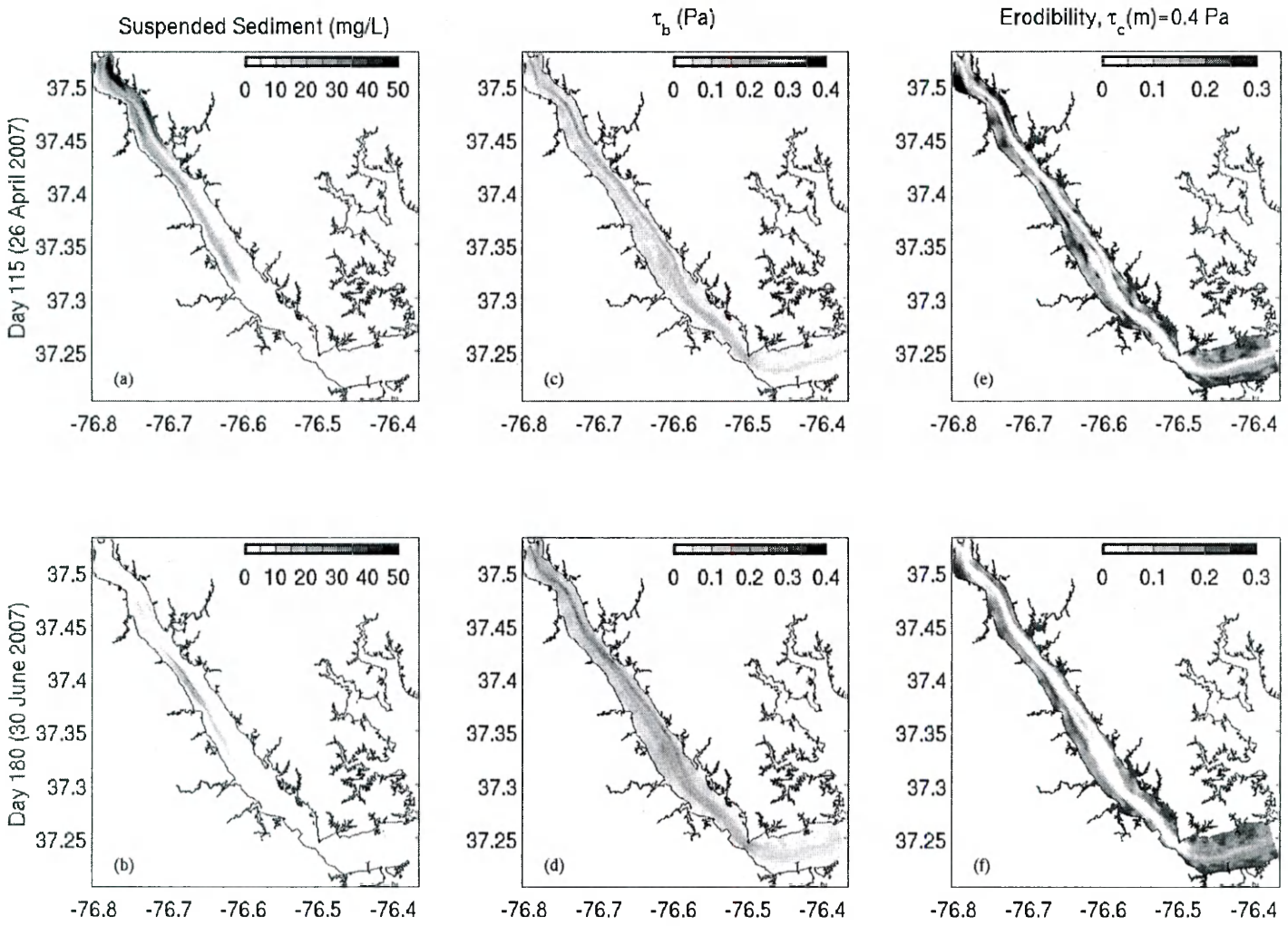

Figure 3.7: Model conditions at day 115, 26 April 2007 (a,c,e) and day 180, 30 June 2007 (b,d,f).(a,b) Depth-averaged suspended sediment concentrations. (c,d) Maximum tidal bed shear stress. (e,f) Erodibility at 0.4 Pa.

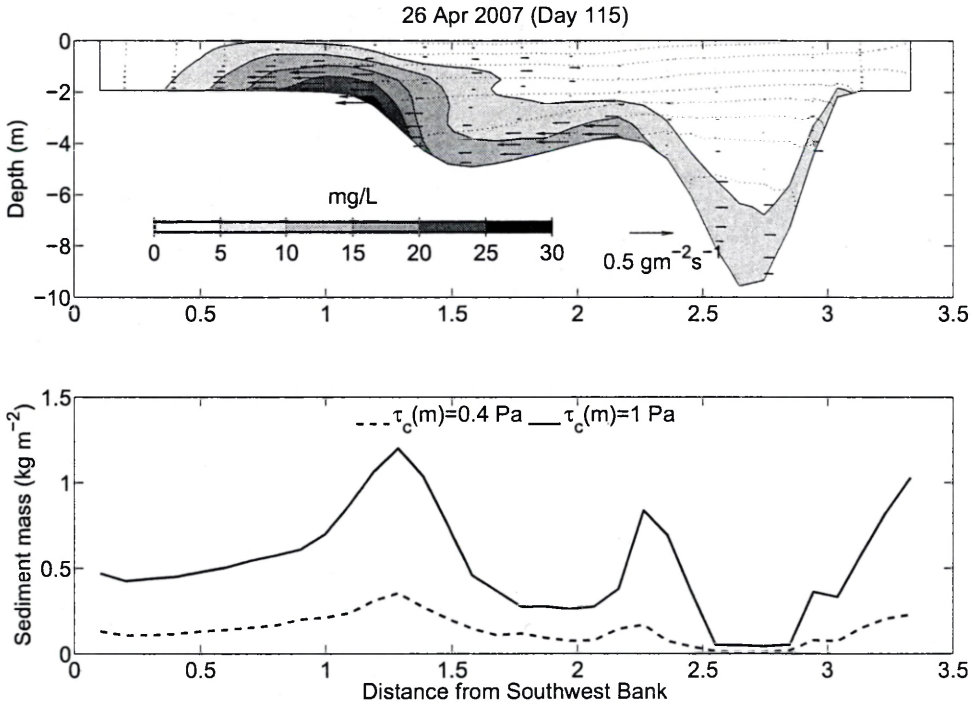

Figure 3.8: Modeled tidally-averaged, cross-channel hydrodynamic and sediment properties at Clay Bank on Day 115 (26 April 2007). (top) (filled contours) Suspended sediment concentrations, (dotted contours) salinty, and (arrows) cross-channel sediment flux at Clay Bank. (bottom) Sediment mass above (dashed) 0.4 Pa and (solid) 1 Pa.

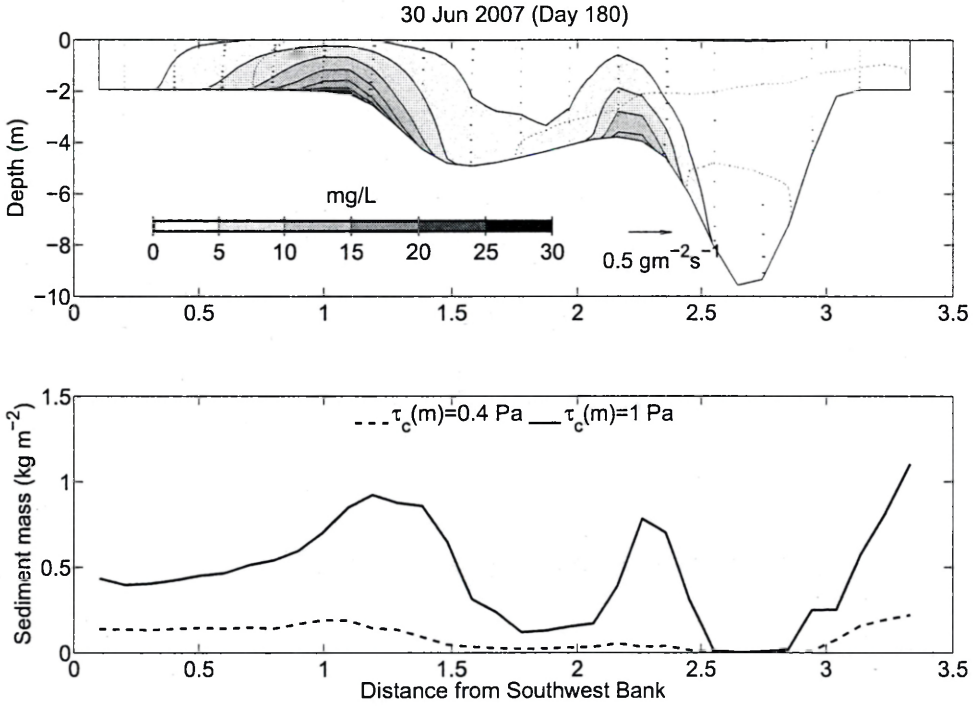

Figure 3.9: Modeled tidally-averaged, cross-channel hydrodynamic and sediment properties at Clay Bank on Day 180 (30 June 2007). (top) (filled contours) Suspended sediment concentrations, (dotted contours) salinity, and (arrows) cross-channel sediment flux. (bottom) Sediment mass above (dashed) 0.4 Pa and (solid) 1 Pa.

importance of bed consolidation was determined through sensitivity tests of the consolidation timescale. Finally, model results were compared to available observations of erodibility and suspended sediment concentrations.

3.6.1 Along-channel sediment fluxes

Along-channel fluxes of sediment in the STM region were evaluated using a box-model type approach, focusing on Clay Bank and the region immediately upriver. (See Figure 3.2). Suspended and bed sediment masses within these regions were integrated and normalized by the regional plan-view area to obtain average values for the region and eliminate cross-channel effects. Total sediment flux into each region was calculated by integrating flux across the region boundaries to quantify movement of sediment along the river.

Tidally-averaged time-series of these calculations are presented in Figure 3.10. As sediment was eroded from the bed during resuspension events triggered by high freshwater flow and spring tides, suspended sediment concentrations increased while bed erodibility decreased. When sediment concentrations fell at the end of a resuspension episode, erodibility increased from deposition of new material to the bed.

At Clay Bank, sediment bed mass decreased slightly from the initial value. During neap tides, reduced bed shear stresses allowed sediment to deposit on the bed, increasing total bed mass and erodibility and reducing fluxes out of the region. Increased sediment erosion on spring tides decreased erodibility and estuarine circulation transported sediment upriver. After 120 days when river flow began to drop, bed mass decreased more steadily at Clay Bank and sediment was lost upriver. By the end of the simulation, sediment bed mass at Clay Bank was slightly below the initial value while erodibility had decreased by 30%.

In the upriver region, sediment was continuously trapped throughout the simulation with greatest fluxes into the region occurring during spring tides. While

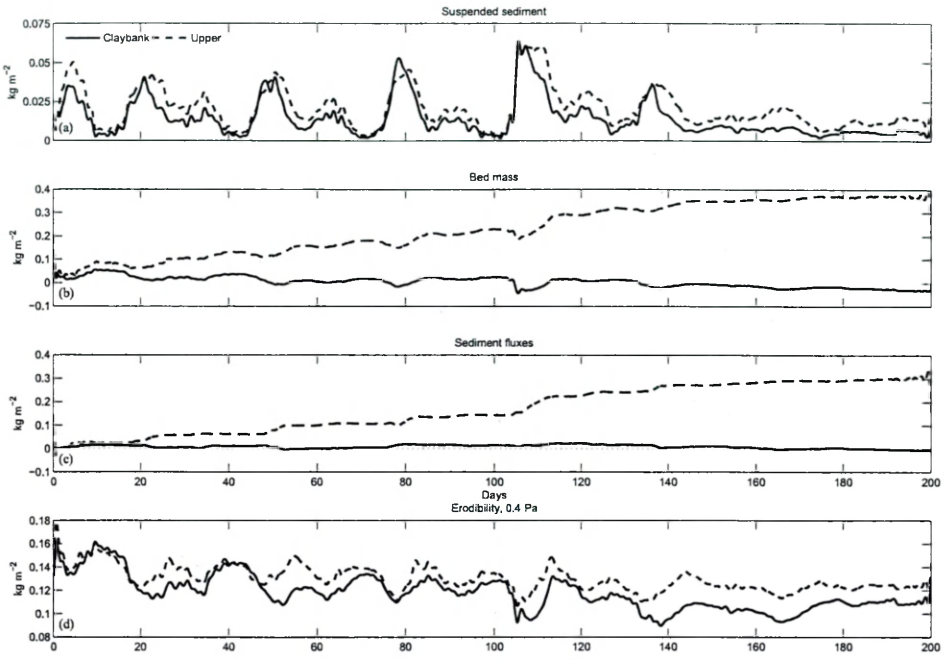

Figure 3.10: Tidally averaged, regionally averaged, sediment concentrations, bed mass, sediment fluxes, and erodibility.(a) Suspended sediment mass for the Clay Bank and Upper River regions. (b) Net change in bed sediment mass since the beginning of the model run. (c) Cumulative sediment flux convergence into the regions . (d) Mean erodibility of the region at $\tau_{cr} = 0.4\,\mathrm{Pa}$ All values are normalized by region area.

fluxes into the region were greater than at Clay Bank, suspended sediment concentrations remained comparable. Most of the sediment transported into the upriver region was deposited on the bed, and the bed mass by the end of the model was eight times the initial mass. Sediment erodibility, however, remained only slightly higher than at Clay Bank, indicating that consolidation decreased erodibility of the newly deposited sediment. While increased fluxes occurred during spring tides which tended to have high sediment concentrations, increased sediment fluxes into the region lag behind the increased sediment concentrations, however. The main source of suspended sediment was therefore locally resuspended material, as further evidenced by the concurrent reduction of bed mass during erosion.

3.6.2 Influence of consolidation timescale T_c

Sensitivity to consolidation timescale T_c on calculations of sediment erodibility and suspended sediment concentrations was investigated. Two additional model runs were completed using different values of T_c: $T_c = 6$ hrs and $T_c = 48$ hrs. Initial conditions and all other parameters were identical to the original model which used $T_c = 24$ hrs. Time-series of these runs are presented with results of the original run in Figure 3.11. Water column sediment concentrations and bed erodibility are only slightly smaller for shorter values of T_c. While the model may not be sensitive to the consolidation timescale, consolidation tests of field collected sediment cores may be able to narrow down the possible consolidation timescales and produce better calculations by allowing initialization techniques like the one used in this study to be more accurate.

This relative insensitivity to consolidation rate is likely explained by model dependence on initial conditions of bed critical stress. A larger spatial coverage of erodibility experiments may be necessary to accurately determine initial bed conditions and improve the model's predictive capabilities. Alternatively, initial bed conditions can be used as a tuning parameter to match observational data.

3.6.3 Comparisons to prior work

The model results were consistent with conclusions from prior research. Dickhudt (2008) presented field observations from sediment cores collected monthly at Clay Bank and Gloucester Point. Similar to his erodibility observations, modeled erodibilities were large in April and May 2007 and decreased the following summer. As in the observations, modeled erodibility at Clay Bank was greater and showed more temporal variability than the relatively constant, low erodibility Gloucester Point site. The model, however, showed large erodibilities at the beginning of the

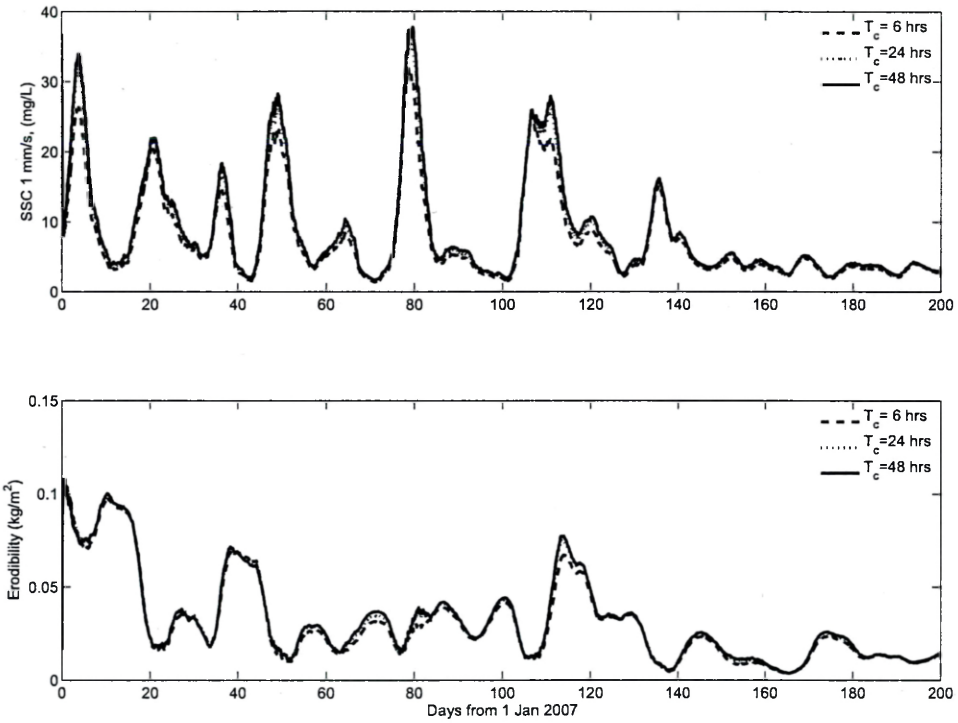

Figure 3.11: Time-series of (top panel) suspended sediment and (bottom panel) erodibility at Clay Bank for $T_c = 6, 24, 48$ hrs. Erodibility is defined as the the bed mass above $\tau_{cr}(m) = 0.4$ Pa

model run in January and another peak around day 40 in mid-February, trends which were not observed by Dickhudt (2008). Being close to the model start, this could be due to the initialization procedure. The model also showed large variations in erodibility during the spring-neap cycle that would not be evident from monthly sediment core observations.

Qualitative similarities also occurred between suspended sediment concentrations calculated by this model and results from previous observational and modeling studies. Transects performed by Lin and Kuo (2001) showed the formation of a single ETM from the convergence of the STM and ETM during high river flows, similar to the modeled results from day 115 (Figure 3.5.) The STM was also located in the same general location as they observed, between 40-50 km upriver of the mouth.

Backscatter observations for cross-channel ADCP transects on 29 March 2007 showed similar qualitative patterns with modeled concentrations (Figure 3.12). While the ADCP backscatter was not calibrated to local suspended sediment concentrations, it provided a comparison to local suspended sediment patterns during the modeled period. The absences of high sediment concentrations in the main channel was seen in both the model and the observations. The model, however, lacked the more well-mixed profiles of the secondary channel and western shoals that was present in the observations and exhibited an area of locally elevated sediment concentrations on the western flank of the secondary channel, which was not apparent in the ADCP observations.

While model results bore some similarities qualitatively, the modeled erodibilities were generally an order of magnitude below the observations. Modeled suspended sediment concentrations were also roughly lower than observations from the river (Lin and Kuo, 2003). This again could result from the choice of initial bed conditions. The available sediment supply assumed at the beginning of the model run may be much lower than actual conditions, reducing both erodibility and suspended

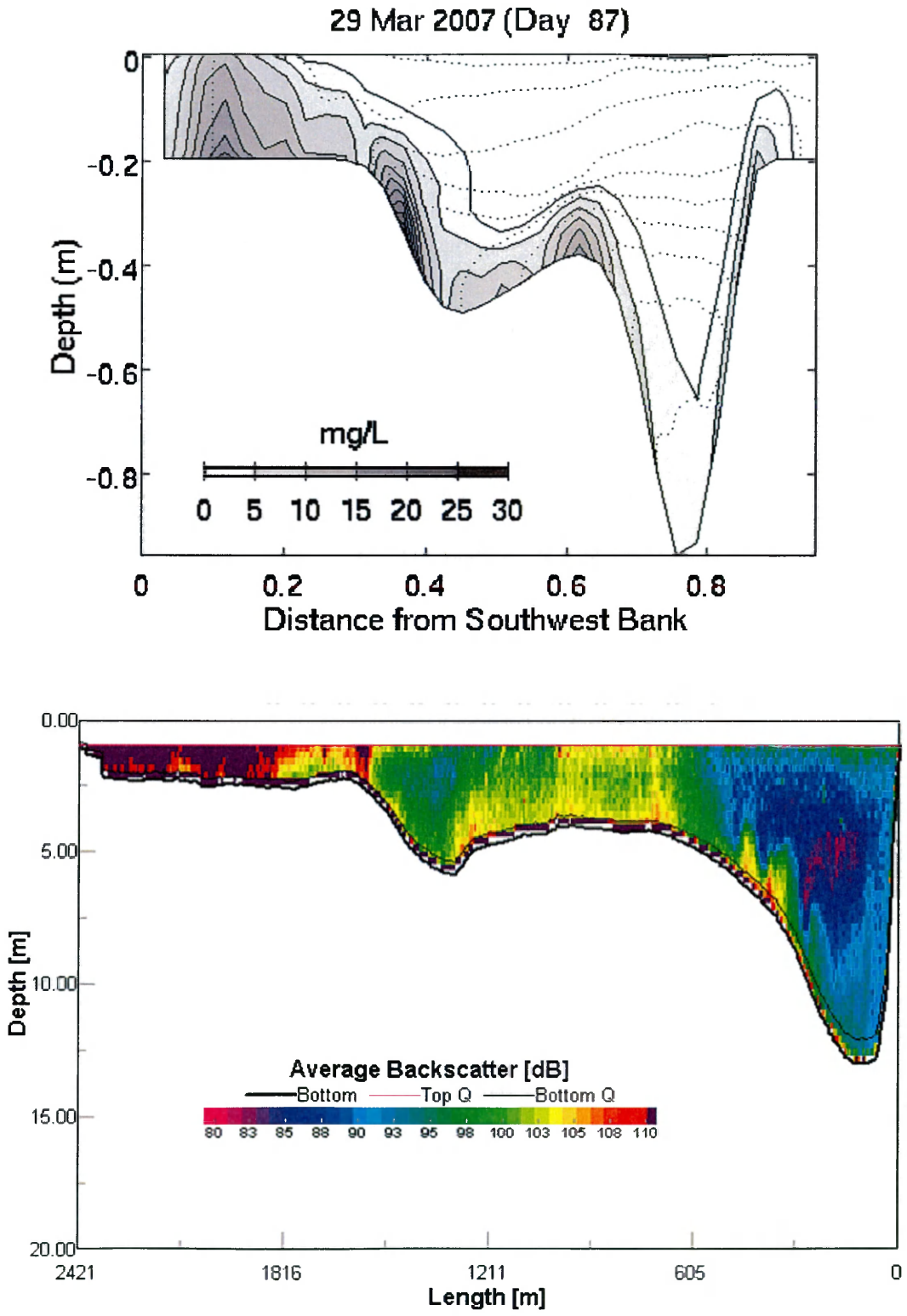

Figure 3.12: Model cross-channel transect versus observations at Clay Bank on 29 March 2007. (top) Model results of (filled contours) suspended sediment concentrations, (dotted contours) salinty, and (arrows) cross-channel velocity. (bottom) ADCP backscatter observations at Clay Bank. ADCP observations are courtesy of Grace Cartwright, VIMS.

sediment concentrations. Alternatively the settling velocities of the sediment size classes may be too high causing sediment to deposit and consolidate rapidly. This would also explain the differences in the vertical distribution of sediment in the cross-channel transects (Figure 3.12). A further possibility is that wave resuspension of sediment on the shoals provides an additional source of sediment to the main river, a process not included in the model.

3.7 Conclusions

Sediment trapping in estuaries is a complex, three-dimensional process that depends on both hydrodynamic and seabed processes. The inclusion of bed consolidation processes by resolving the vertical structure and temporal behavior of τ_{cr} is a promising method for modeling cohesive sediment processes. This Chapter has demonstrated the following:

1. Magnitudes of local suspended sediment concentrations in the York River mainly responded to variations in seabed erodibility while patterns of spatial variability were dependent on convergent sediment transport processes.

2. By the end of the modeled time-period, sediment was removed from the Clay Bank region and redeposited upriver. Most upriver sediment transport occurred during times of high freshwater flow and spring tides.

3. STM dynamics in the Clay Bank region were three dimensional with greatest sediment concentrations on the channel flanks and shoals. Cross-channel sediment trapping processes were important for understanding sediment trapping processes in this region.

4. Physical processes like bed consolidation and variability in sediment flux convergence and divergence were important in the creation of seasonal patterns

of erodibility.

In summary, this model is an important tool to aid our understanding of sediment transport in the York River Estuary. Complex feedbacks between sediment erodibility, suspended sediment, and sediment trapping are inherently three-dimensional. Numerical models allow for spatial and temporal resolutions that cannot be observed using available technologies and provide us greater understanding of the processes involved.

CHAPTER 4

Conclusions

This thesis has presented the results of incorporating a cohesive sediment bed model into ROMS and its use in a simulation of the York River Estuary. The sensitivity of model calculations to critical stress profiles and consolidation timescales were tested. The evolution of bed erodibility over 200 days was observed using the results of the York River model. Feedbacks between bed erodibility and suspended sediment concentrations were shown to be important to sediment dynamics in the estuary.

Chapter 2 focused on the importance of bed sediment erodibility in determining suspended sediment concentrations using a one-dimensional model of the water column and seabed. Analysis of erodibility observations of sediment cores showed that sediment erodibility is primarily depth-limited (Type I) under typical tidal conditions. Depth limitation is further supported by modeled erodibility experiments using a constant erosion rate that agreed well with observations. For York River sites, seasonal variations in critical shear stress impacted suspended sediment magnitudes by a factor of 2.5.

Model sensitivity tests to consolidation timescales showed that increasing the timescale from hours to days caused similar changes in sediment concentrations observed between spring and neap tides. The results of this analysis suggest that sediment critical shear stresses and consolidation are as important as tidal bed stresses

in controlling suspended sediment concentrations. The effects of long consolidation timescales also created an asymmetry in sediment concentrations as sediment recently suspended during spring tides was unable to consolidate quickly and remained more easily erodible than prior to the spring tide. Thus the consolidation timescale influenced suspended sediment concentrations both qualitatively, by creating an asymmetry around spring tide,and quantitatively, by increasing sediment erodibility and therefore water column concentrations.

Chapter 3 examined the use of the bed model within a three-dimensional simulation of the York River for the first 200 days of 2007. Modeled erodibilities at Clay Bank were generally greater than those at Gloucester Point. The estimated Clay Bank erodibilities also exhibited significant temporal variations. The largest erodibilities occurred during neap tides after increased sediment settling and during periods of high river flow. Spatially, erodibility and suspended sediment concentrations were correlated, with highly erodible areas exhibiting high suspended sediment concentrations. The channel flanks and shoals evolved to have the most highly erodible areas while the main channels became scoured of erodible sediment and exhibited low suspended sediment concentrations. This indicated that sediment erodibility can be a primary factor in determining sediment concentrations while hydrodynamic processes contribute to the spatial distributions of highly erodible sediment.

Analysis of along-channel fluxes showed that the Clay Bank region is a convergence zone only during spring tides and high river flows. The largest upriver sediment fluxes occurred during spring tides when water-column sediment concentrations and residual circulation were greatest. As flows diminished, sediment fluxed out of the Clay Bank region and upriver toward the primary ETM mainly during spring tides. Sediment erodibilities began to fall with decreasing river flow as sediment was removed from the Clay Bank area. The modeled estimates of concentra-

tion and erodibility were less sensitive to the consolidation rate than to the initial sediment distribution.

While the three-dimensional model was qualitatively similar to conditions observed in the York River, future work should focus on improving the accuracy of calculations. Observations of suspended sediment concentrations and settling velocities during the modeled time period were unavailable for model calibration. Such observations, when available, would allow the model to be tuned to more closely resemble the estuary.

Additionally, inclusion of the effects of winds and waves may add to the realism of the model. Waves may be important in resuspending sediment from the shoals an allowing redistribution to other areas of the river. Wave resuspension, however, is likely unimportant in the channel due to the greater depths. Winds may temporarily alter hydrodynamics, causing short-term changes in both along and across channel sediment convergence. Both processes may increase the supply of sediment in the channel.

Due to the spatial complexity of the model, better methods of bed initialization need to be explored. Greater spatial coverage of erodibility observations would help constrain critical shear stress parameters while consolidation tests would more accurately determine the consolidation and swelling timescales. The influence of the swelling timescale was not explored though this may be an important factor in generating erodible sediment in the scoured main channels.

This study is among the first to apply the bed model of Sanford (2008) to a one-dimensional model and a more realistic three-dimensional case and represents an important step for the Comunity Sediment Transport Modeling System. By including consolidation and depth-variations in critical stress within the York River model it has shown that bed erodibility evolves based on the manner in which hydrodynamic forcing controls sediment flux convergences and divergences. Likewise,

sediment concentrations in the water column respond to seabed erodibility so that a complex feedback exists between sediment bed availability, concentrations, and flux convergence. Such feedbacks are likely important to other estuarine systems and also to other depositional environments.

BIBLIOGRAPHY

Black, K. (1997). Microbiological factors contributing to erosion resistance in natural cohesive sediments. In Burt, Parker, and Watts, editors, *Cohesive Sediments*, pages 231–244. Wallingford, UK.

Boudreau, B. P. and Jorgensen, B. B., editors (2001). *The Benthic Boundary Layer: Transport Processes and Biogeochemistry.* Oxford University Press, New York.

Dellapenna, T. M., Kuehl, S. A., and Schaffner, L. C. (2003). Ephemeral deposition, seabed mixing and fine-scale strata formation in the York River estuary, Chesapeake Bay. *Estuarine, Coastal and Shelf Science*, 58(3):621–643.

Dellappenna, T., Kuehl, S., and Schaffner, L. (1998). Sea-bed mixing and particle residence times in biologically and physically dominated estuarine systems: A comparison of Lower Chesapeake Bay and the York River subestuary. *Estuarine, Coastal and Shelf Science*, 46(6):777–795.

Dennison, W. C., Orth, R. J., Moore, K. A., Stevenson, J. C., Carter, V., Kollar, S., Bergstrom, P. W., and Batiuk, R. A. (1993). Assessing water quality with submersed aquatic vegetation. *Bioscience*, 43(2):86–94.

Dickhudt, P. (2008). Controls on erodibility in a partially mixed estuary: York river, va. Master's thesis, School of Marine Science, College of William and Mary, Gloucester Point, VA.

Dickhudt, P., Friedrichs, C., and Sanford, L. (2008). Mud matrix solids fraction and bed erodibility in the York River, USA and other muddy environments. In *Proceedings of the 9th International Conference of Nearshore and Estuarine Cohesive Sediment Transport Processes, 2007.* submitted.

Drake, D. E., EganHouse, R., and McArther, W. (2002). Physical and chemical effects of grain aggregates on the Palos Verdes margin, southern California. *Continental Shelf Research*, 22(6-7):967–986.

Dyer, K. (1995). Sediment transport processes in estuaries. In Perillo, G., editor, *Geomorphology and Sedimentology of Estuaries*, pages 423–449. Elsevier.

Ferre, B. and Sherwood, C. (2007). Evaluation of sediment resuspension and transport over a mixed-bed with ROMS. In *9th International Conference of Nearshore and Estuarine Cohesive Sediment Transport Processes*, Brest, France.

Festa, J. F. and Hansen, D. V. (1978). Turbidity maxima in partially mixed estuaries: A two-dimensional numerical model. *Estuarine and Coastal Marine Science*, 7:347–359.

Friedrichs, C., Armbrust, B., and de Swart, H. (1998). Hydrodynamics and equilibrium sediment dynamics of shallow, funnel-shaped tidal estuaries. In Dronkers, J. and Scheffers, M., editors, *Physics of Estuaries and Coastal Seas*, pages 315–328, Rotterdam, The Netherlands. Balkema Press.

Fugate, D. C. and Friedrichs, C. T. (2003). Controls on suspended aggregate size in partially mixed estuaries. *Estuarine, Coastal and Shelf Science*, 58:389–404.

Gailani, J., Ziegler, C. K., and Lick, W. (1991). Transport of suspended solids in the lower Fox River. *Journal of Great Lakes Research*, 17(4):479–494.

Geyer, W. R. (1993). The importance of suppression of turbulence by stratification on the estuarine turbidity maximum. *Estuaries*, 16(1):113–125.

Geyer, W. R., Woodruff, J. D., and Traykovski, P. (2001). Sediment transport and trapping in the Hudson River Estuary. *Estuaries*, 24(5):670–679.

Gibson, R., England, G., and Hussey, M. (1967). The theory of one-dimensional consolidation of saturated clays. *Geotechnique*, 17:261–273.

Gularte, R., Kelly, W., and Nacci, V. (1980). Erosion of cohesive sediments as a rate process. *Ocean Engineering*, 7:539–551.

Gust, G. and Muller, V. (1997). Interfacial hydrodynamics and entrainment functions of currently used erosion devices. In Burt, Parker, and Watts, editors, *Cohesive Sediments*, pages 149–174. Wallingford, U.K.

Haidvogel, D., Arango, H., Budgell, W., Cornuelle, B., Curchitser, E., Di Lorenzo, E., Fennel, K., Geyer, W., Hermann, A., Lanerolle, L., Levin, J., McWilliams, J., Miller, A., Moore, A., Powell, T., Shchepetkin, A., Sherwood, C., Signell, R., Warner, J., and Wilkin, J. (2008). Ocean forecasting in terrain-following coordinates: Formulation and skill assessment of the Regional Ocean Modeling System. *Journal of Computational Physics*, 227:3595–3624.

Haidvogel, D. B. and Beckmann, A. (1999). *Numerical Ocean Circulation Modeling.* Imperial College Press, London.

Harris, C. K., Traykovski, P. A., and Geyer, W. R. (2004). Flood dispersal and deposition by near-bed gravitational sediment flows and oceanographic transport: A numerical modeling study of the Eel River shelf, northern California. *Journal of Geophysical Research*, 110:C09025, doi:10.1029 / 2004JC002727.

Harris, C. K. and Wiberg, P. L. (1997). Approaches to quantifying long-term continental shelf sediment transport with an example from the Northern California STRESS mid-shelf site. *Continental Shelf Research*, 17(11):1389–1418.

Harris, C. K. and Wiberg, P. L. (2001). A two-dimensional, time-dependent model of suspended sediment transport and bed reworking for continental shelves. *Computers & Geosciences*, 27(6):675–690.

Hill, P. S. and McCave, I. (2001). *Suspended Particle transport in benthic boundary layers*, pages 78–103. In Boudreau and Jorgensen (2001).

HydroQual, Inc (2002). ECOM-SED v1.3 Users Manual. Mahwah, NJ.

Jay, D. A. and Musiak, J. D. (1994). Particle trapping in estuarine tidal flows. *Journal of Geophysical Research*, 99(C10):20445–20461.

Kniskern, T. and Kuehl, S. (2003). Spatial and temporal variability of seabed disturbance in the York River subestuary. *Estuarine, Coastal, and Shelf Science*, 58:37–55.

Koch, E. W. (2001). Beyond light: Physical, geological, and geochemical parameters as possible sumbmersed aquatic vegetation habitat requirements. *Estuaries*, 24(1):1–17.

Kwon, J.-I. (2005). *Simulation of turbidity maximums in the York River, Virginia.* PhD thesis, The College of William and Mary.

Lang, G., Schubert, R., Markofsky, M., Fanger, H.-U., Grabemann, I., Krasemann, H., Neumann, L., and Riethmüller, R. (1989). Data interpretation and numerical modeling of the mud and suspended sediment experiment 1985. *Journal of Geophysical Research*, 94(C10):14381–14393.

Lick, W. (1982). The transport of contaminants in the Great Lakes. *Annual Review of Earth and Planetary Sciences*, 10:327–353.

Lick, W., Lick, J., and Ziegler, C. K. (1994). The resuspension and transport of fine-grained sediments in Lake Erie. *Journal of Great Lakes Research*, 20(4):599–612.

Lin, J. and Kuo, A. Y. (2001). Secondary turbidity maximum in a partially mixed microtidal estuary. *Estuaries*, 24(5):707–720.

Lin, J. and Kuo, A. Y. (2003). A model study of turbidity maxima in the York River Estuary, Virginia. *Estuaries*, 26(5):1269–1280.

Maa, J. P.-Y. and Kim, S.-C. (2002). A constant erosion rate model for fine sediment in the York River, Virginia. *Environmental Fluid Mechanics*, 1:345–360.

Maa, J. P.-Y., Sanford, L. P., and Halka, J. P. (1998). Sediment resuspension characteristics in Baltimore Harbor, Maryland. *Marine Geology*, 146:137–145.

McLean, S. (1985). Theoretical modelling of deep ocean sediment transport. *Marine Geology*, 115(3/4):271–287.

McNeil, J., Taylor, C., and Lick, W. (1996). Measurements of erosion of undisturbed bottom sediments with depth. *Journal of Hydraulic Engineering*, 122(6):316–324.

Mellor, G. L. and Yamada, T. (1982). Development of a turbulence closure model for geophysical fluid problems. *Reviews of Geophysics and Space Physics*, 20(4):851–875.

Nichols, M., Kim, S., and Brouwer, C. (1991). Sediment characterization of the Chesapeake Bay and its tributaries, Virginian province. NOAA National Estuarine Inventory: Supplement.

Parchure, T. M. and Mehta, A. J. (1985). Erosion of soft cohesive sediment deposits. *Journal of Hydraulic Engineering*, 111(10):1308–1326.

Park, K., Kuo, A., Shen, T., and Hamrick, J. (1995). A three dimensional hydrodynamic-eutrophication model (HEM-3D): Description of water quality and sediment process submodels. Technical Report 327, Virginia Institute of Marine Science, The College of William and Mary, Gloucester Point, Virginia. Special report in Applied Marine Science and Ocean Engineering.

Piedra-Cueva, I. and Mory, M. (2001). Erosion of a deposited layer of cohesive sediment. In McAnally, W. and Mehta, A., editors, *Coastal and Estuarine Fine Sediment Transport*, pages 41–52. Elsevier, Amsterdam.

Postma, H. (1967). Sediment transport and sedimentation in the estuarine environment. American Association for the Advancement of Science, Washington, DC.

Roberts, J., Jepsen, R., Gotthard, D., and Lick, W. (1998). Effects of particle size and bulk density of erosion of quartz particles. *Journal of Hydraulic Engineering*, 124(12):1261–1268.

Roberts, W. and Pierce, J. (1976). Deposition in the upper Patuxent Estuary, Maryland,1968-1969. *Estuarine and Coastal Marine Science*, 4:267–280.

Sanford, L. P. (2006). Uncertainties in sediment erodability estimates due to a lack of standards for experimental protocols and data interpretation. *Integrated Environmental Assessment and Management*, 2(1):29–34.

Sanford, L. P. (2008). Modeling a dynamically varying mixed sediment bed with erosion, deposition, bioturbation, consolidation, and armoring. *Computers and Geosciences*, 34(10):1263–1283.

Sanford, L. P. and Maa, J. P.-Y. (2001). A unified erosion formulation for fine sediments. *Marine Geology*, 179:9–23.

Sanford, L. P., Suttles, S. E., and Halka, J. P. (2001). Reconsidering the physics of the Chesapeake Bay estuarine turbidity maximum. *Estuaries*, 24(5):655–669.

Schaffner, L., Dickhut, R., Mitra, S., Lay, P., and Brouwer-Riel, C. (1997). Effects of physical chemistry and bioturbation by estuarine macrofauna on the transport of hydrophobic organic contaminants in the benthos. *Environmental Science and Technology*, 31:3120–3125.

Schaffner, L. C., Dellapena, T. M., Hinchey, E. K., Friedrichs, C. T., Neubauer, M. T., Smith, M. E., and Keuhl, S. A. (2001). Physical energy regimes, seabed dynamics, and organism-sediment interactions along an estuarine gradient. In Aller, J. Y., Woodin, S. A., and Aller, R., editors, *Organism-Sediment Interactions*, pages 159–179. University of South Carolina Press, Columbia, SC.

Schoellhamer, D. (2001). Influence of salinity, bottom topography, and tides on locations of estuarine turbidity maxima in northern San Fransisco Bay. In *Coastal and Estuarine Fine Sediment Processes*. Elsevier.

Schubel, J. (1968). Turbidity maximum of the northern chesapeake bay. *Science*, 161(3845):1013–1015.

Scully, M., Friedrichs, C., and Wright, L. (2003). Numerical modeling of gravity-driven sediment transport and deposition on an energetic continental

shelf: Eel River, northern California. *Journal of Geophysical Research*, 108(C4):3120.

Scully, M. E. and Friedrichs, C. T. (2007). Sediment pumping by tidal asymmetry in a partially mixed estuary. *Journal of Geophysical Research*, 112:C07028, doi:10.1029/2006JC003784.

Shchepetkin, A. F. and McWilliams, J. C. (2005). The Regional Oceanic Modeling System (ROMS): a split-explicit, free-surface, topography-following-coordinate oceanic model. *Ocean Modelling*, 9:347–404.

Sherwood, C., Ferre, B., and Murray, C. (2007). Cohesive sediment erodibility and evolution of a sandy mud deposit on the Palos Verdes shelf, USA. In *9th International Conference of Nearshore and Estuarine Cohesive Sediment Transport Processes*, Brest, France.

Sherwood, C., Harris, C., Geyer, W., and Butman, B. (2002a). Toward a community coastal sediment transport modeling system: The second workshop. *EOS Trans. AGU*, 83(51):604.

Sherwood, C. R., Drake, D. E., Wiberg, P. L., and Wheatcroft, R. A. (2002b). Prediction of the fate of p,p'-DDE in sediment on the Palos Verdes shelf, California, USA. *Continental Shelf Research*, 22:1025–1058.

Shields, A. (1936). Anwendung der aehnlichkeitsmechanik und der turbulenzforschung auf die geschiebebewegung. *Mitteilungen der Preussischen Versuchsanstalt fur Wasserbau und Schiffbau*, 26:5–24. [English title: Application of similarity principles and turbulence research to bed-load movement. Translation by Ott, W.P. and J.C. van Uchelen, Technical Report, California Institute of Technology, Hydrodynamics Lab, Publication 167].

Smolarkiewicz, P. K. and Margolin, L. G. (1998). Mpdata: A finite-difference solver for geophysical flows. *Journal of Computational Physics*, 140:459–480.

Stevens, A., Wheatcroft, R., and Wiberg, P. (2007). Seabed properties and sediment erodibility along the western Adriatic margin, Italy. *Continental Shelf Research*, 27:400–416.

Thomsen, L. and Gust, G. (2000). Sediment erosion thresholds and characteristics of resuspended aggregates on the western European continental margin. *Deep-Sea Research*, 47:1881–1897.

Toorman, E. and Berlamont, J. (1993). Mathematical modeling of cohesive sediment settling and consolidation. In Mehta, A., editor, *Nearshore and Estuarine Cohesive Sediment Transport*, pages 167–184. American Geophysical Union, Washington, DC.

Uncles, R. J. and Stephens, J. A. (1989). Distributions of suspended sediment at high water in a macrotidal estuary. *Journal of Geophysical Research*, 94(C10):14395–14405.

van Ledden, M., van Kesteren, W., and Winterwerp, J. (2004). A conceptual framework for the erosion behavior of sand-mud mixtures. *Continental Shelf Research*, 24:1–11.

Wang, X. and Pinardi, N. (2002). Modeling the dynamics of sediment transport and resuspension in the northern Adriatic Sea. *Journal of Geophysical Research*, 107(C12):doi:10.1029/2001JC001303.

Warner, J., Geyer, W., and Lerczak, J. (2005). Numerical modeling of an estuary: A comprehensive skill assessment. *Journal of Geophysical Research*, 110:C05001.

Warner, J., Sherwood, C., Signell, R., Harris, C., and Arango, H. (2008). Development of a three-dimensional, regional, coupled wave-, current-, and sediment-transport model. *Computers and Geosciences*, 34(10):1284–1306.

Warner, J. C., Sherwoord, C. R., and Geyer, W. R. (2007). Sensitivity of estuarine turbidity maximum to settling velocity, tidal mixing, and sediment supply. In Maa, J.-Y., Sanford, L., and Schoellhamer, D., editors, *Estuarine and Coastal Fine Sediment Dynamics*, volume 8 of *Proceedings in Marine Science*, pages 355–375, Amsterdam, The Netherlands. Elsevier B.V.

Wellershaus, S. (1981). Turbidity maximum and mud shoaling in the Weser Estuary. *Archiv fuer Hydrobiologie*, 92(2):161–198.

Wiberg, P. L., Drake, D. E., and Cacchione, D. (1994). Sediment resuspension and bed armoring during high bottom stress events on the northern California inner continental shelf: measurements and predictions. *Continental Shelf Research*, 14(10-11):1191–1219.

Wiberg, P. L. and Harris, C. K. (2002). Desorption of p,p';-DDE from sediment during resuspension events on the Palos Verdes shelf, California: a modeling approach. *Continental Shelf Research*, 22(6-7):1005–1023.

Wiberg, P. L. and Smith, J. D. (1987). Calculations of critical shear stress for motion of uniform and heterogeneous sediments. *Water Resources Research*, 23(8):1471–1480.

Winterwerp, J. and van Kesteren, G. (2004). *Introduction to the Physics of Cohesive Sediment in the Marine Environment.* Developments in Sedimentology. Elsevier.

Woodruff, J. D., Geyer, W. R., Sommerfield, C. K., and Driscoll, N. W. (2001). Seasonal variation of sediment deposition in the hudson river estuary. *Marine Geology*, 179:105–119.

VITA

Jeffrey Paul Rinehimer

Born 1 May 1982 in Lititz, PA. Graduated from Warwick Senior High School, 2000. Earned a B.S. in Environmental Geoscience from Boston College in 2004. Entered the M.S. program in Marine Science at the School of Marine Science, The College of William and Mary in 2004.